U. S. Department of Commerce
National Oceanic and Atmospheric Administration
National Weather Service
National Centers for Environmental Prediction

Office Note 414

Initial Results from Long-Term Measurements of Atmospheric Humidity and Related Parameters in the Marine Boundary Layer at Two Locations in the Gulf of Mexico[1]

Laurence C. Breaker[2], David B. Gilhousen[3],
Hendrik L. Tolman[4] and Lawrence D. Burroughs[2]

June 1996

---

[1]OPC Contribution Number 124

[2]NOAA/National Weather Service, NCEP, Washington, D.C. 20233
[3]NOAA/National Weather Service, Data Buoy Center, Stennis Space Center, MS 39529
[4]UCAR Visiting Scientist

OPC CONTRIBUTIONS

No. 1. Burroughs, L. D., 1987: Development of Forecast Guidance for Santa Ana Conditions. National Weather Digest, Vol. 12 No. 1, 7pp.

No. 2. Richardson, W. S., D. J. Schwab, Y. Y. Chao, and D. M. Wright, 1986: Lake Erie Wave Height Forecasts Generated by Empirical and Dynamical Methods -- Comparison and Verification. Technical Note, 23pp.

No. 3. Auer, S. J., 1986: Determination of Errors in LFM Forecasts Surface Lows Over the Northwest Atlantic Ocean. Technical Note/NMC Office Note No. 313, 17pp.

No. 4. Rao, D. B., S. D. Steenrod, and B. V. Sanchez, 1987: A Method of Calculating the Total Flow from A Given Sea Surface Topography. NASA Technical Memorandum 87799., 19pp.

No. 5. Feit, D. M., 1986: Compendium of Marine Meteorological and Oceanographic Products of the Ocean Products Center. NOAA Technical Memorandum NWS NMC 68, 93pp.

No. 6. Auer, S. J., 1986: A Comparison of the LFM, Spectral, and ECMWF Numerical Model Forecasts of Deepening Oceanic Cyclones During One Cool Season. Technical Note/NMC Office Note No. 312, 20pp.

No. 7. Burroughs, L. D., 1987: Development of Open Fog Forecasting Regions. Technical Note/NMC Office Note. No. 323., 36pp.

No. 8. Yu, T. W., 1987: A Technique of Deducing Wind Direction from Satellite Measurements of Wind Speed. Monthly Weather Review, 115, 1929-1939.

No. 9. Auer, S. J., 1987: Five-Year Climatological Survey of the Gulf Stream System and Its Associated Rings. Journal of Geophysical Research, 92, 11,709-11,726.

No. 10. Chao, Y. Y., 1987: Forecasting Wave Conditions Affected by Currents and Bottom Topography. Technical Note, 11pp.

No. 11. Esteva, D. C., 1987: The Editing and Averaging of Altimeter Wave and Wind Data. Technical Note, 4pp.

No. 12. Feit, D. M., 1987: Forecasting Superstructure Icing for Alaskan Waters. National Weather Digest, 12, 5-10.

No. 13. Sanchez, B. V., D. B. Rao, and S. D. Steenrod, 1987: Tidal Estimation in the Atlantic and Indian Oceans. Marine Geodesy, 10, 309-350.

No. 14. Gemmill, W. H., T. W. Yu, and D. M. Feit 1988: Performance of Techniques Used to Derive Ocean Surface Winds. Technical Note/NMC Office Note No. 330, 34pp.

No. 15. Gemmill, W. H., T. W. Yu, and D. M. Feit 1987: Performance Statistics of Techniques Used to Determine Ocean Surface Winds. Conference Preprint, Workshop Proceedings AES/CMOS 2nd Workshop of Operational Meteorology. Halifax, Nova Scotia., 234-243.

No. 16. Yu, T. W., 1988: A Method for Determining Equivalent Depths of the Atmospheric Boundary Layer Over the Oceans. Journal of Geophysical Research. 93, 3655-3661.

No. 17. Yu, T. W., 1987: Analysis of the Atmospheric Mixed Layer Heights Over the Oceans. Conference Preprint, Workshop Proceedings AES/CMOS 2nd Workshop of Operational Meteorology, Halifax, Nova Scotia, 2, 425-432.

No. 18. Feit, D. M., 1987: An Operational Forecast System for Superstructure Icing. Proceedings Fourth Conference Meteorology and Oceanography of the Coastal Zone. 4pp.

No. 19. Esteva, D. C., 1988: Evaluation of Priliminary Experiments Assimilating Seasat Significant Wave Height into a Spectral Wave Model. Journal of Geophysical Research. 93, 14,099-14,105.

No. 20. Chao, Y. Y., 1988: Evaluation of Wave Forecast for the Gulf of Mexico. Proceedings Fourth Conference Meteorology and Oceanography of the Coastal Zone, 42-49.

ABSTRACT

Measurements of boundary layer moisture have been acquired from Rotronic MP-100 sensors deployed on two NDBC buoys in the northern Gulf of Mexico from June through November 1993. For one sensor which was retrieved approximately 8 months after deployment, the post- and pre-calibrations agreed closely and fell well within WMO specifications for accuracy. Buoy observations of relative humidity and supporting data were used to calculate specific humidity, and the surface fluxes of latent and sensible heat. Specific humidities from the buoys were compared with observations of moisture obtained from nearby ship reports and the correlations were generally high (0.7 - 0.9). These data were not sufficient, however, to confirm or refute a recent report of hysteresis that may occur with the Rotronic sensor.

The time series of specific humidity and the other buoy parameters revealed three primary scales of variability, small-scale (of the order of hours), synoptic-scale (several days), and seasonal (several months). The synoptic-scale variability was clearly dominant; it was event-like in character and occurred primarily during September, October, and November. Most of the synoptic-scale variability was due to frontal systems that dropped down into the Gulf of Mexico from the continental U.S., followed by air masses which were cold and dry. Cross-correlation analyses of the buoy data indicated that both specific humidity and air temperature served as tracers of the motion associated with propagating atmospheric disturbances. Spectra of the various buoy parameters indicated strong diurnal and semidiurnal variability for barometric pressure and sea surface temperature (SST) and lesser variability for air temperature and wind speed.

The calculated surface fluxes of latent and sensible heat were dominated by the synoptic events which took place from September through November. Mean Bowen ratios were in the range 6 - 8%, indicating that the latent heat fluxes far exceeded the sensible heat fluxes in this region. Finally, an analysis of the surface wave observations from each buoy, which included calculations of wave age and estimates of surface roughness, yielded results which are consistent with enhanced moisture exchange between the ocean and the marine boundary layer during periods of high latent heat flux.

1. INTRODUCTION

The acquisition of meteorological observations within the marine boundary layer has always posed unique problems due to the proximity of the ocean surface to the sensor location, and the constant state of motion of the surface itself. Atmospheric humidity has been a particularly difficult parameter to measure near the ocean surface. First, it is difficult to protect humidity sensors from salt spray which accumulates over time and consequently degrades calibration accuracy; second, humidity sensors must be adequately protected excess heating due to incoming solar radiation; and finally, humidity sensors must recover from periods of saturation rapidly and without change to their calibration (Coantic and Friehe 1980).

Since atmospheric moisture is a difficult parameter to measure accurately over the ocean, it is not surprising that it has been even more difficult to acquire observations of boundary layer moisture from unattended instruments for extended periods of several months or more. Recently, however, a number of humidity sensors have been evaluated for possible use in measuring atmospheric moisture in the marine environment (*e.g.*, Semmer 1987; Muller and Beekman 1987; Crescenti *et al.* 1990; Katsaros *et al.* 1994).

Because of the continuing need for long-term measurements of moisture within the marine boundary layer, the National Data Buoy Center (NDBC) evaluated the Rotronic MP-100 humidity sensor for possible deployment on their moored ocean data buoys, based on promising test results from Muller and Beekman (1987) and Semmer (1987). Initial field tests were conducted along the U.S. West Coast in 1989. A Rotronic humidity sensor was installed on a Coastal-Marine Automated Network (C-MAN) station at Point Arguello, California and showed high correlations between saturation events and restricted visibilities in fog. Calculated dew point temperatures following fog events were in general agreement with those reported at Vandenberg Air Force Base located nearby. After a four-month evaluation, Rotronic humidity sensors were introduced on several NDBC buoys and C-MAN stations along the California coast, but, initially, several gross failures occurred within weeks after they were installed. A gross failure occurred when reported relative humidities either:

- (1) exceeded 106%,
- (2) remained at, or exceeded, 100% for a day or more after satellite imagery indicated fog dissipation, or
- (3) disagreed by 30% or more with nearby reports for low values typically less then 30%.

These failures lead to several improvements to the Rotronic sensor and its installation aboard the NDBC buoy platforms.

- First, the cabling from the sensor to the on-board electronic payload was replaced. The original cables had inadequate insulation and cable flexing often produced large calibration shifts.

- Second, the method of calibration was changed by exposing the sensor to a series of different saturated salt solutions in closed flasks and then comparing the observed relative humidities to the known equilibrium vapor pressure of water at the observed temperatures for these solutions.

Test flasks with relative humidities ranging from 11 to 96% were used. These improvements led to significantly greater measurement accuracy and sensor reliability. As a result, these instruments have been installed on a number of NDBC buoys since 1989, concomitant with improvements in their performance.

As a basis for this study, we acquired hourly measurements of relative humidity and other supporting environmental data from two NDBC buoys in the Gulf of Mexico (Fig. 1) which were equipped with the improved Rotronic MP-100 humidity sensors for the period 5 June to 30 November 1993. Initially, details of the sensor calibration, deployment and reliability are addressed. Then the relative humidity and supporting data from the buoys are used to calculate specific humidity and the corresponding fluxes of latent and sensible heat. To provide a measure of validation for these observations, the moisture data are compared with reports from nearby ships and other fixed platforms. A number of synoptic events occurred during the measurement period which provided an opportunity to examine the response of the instrument to these events.

2. INSTRUMENT DESCRIPTION

a. Background

The Rotronic MP-100 humidity sensor has been under development since about 1980. Although the initial design was fragile and susceptible to contamination (Crane and Boole 1988), recent versions of the instrument have proven more rugged and less sensitive to contamination. The Rotronic MP-100 is classified as a thin film capacitive polymer sensor (Crescenti *et al.* 1990). The operation of the instrument's transducer is based on the principle of capacitance change as the polymer absorbs and desorbs water vapor. A Gor-Tex filter covers the transducer and allows water vapor (but not liquid water) to pass through it. Contaminants reduce the passage of water vapor through the filter which can lead to erroneous reports of saturation following high moisture events. As a result, the filter must be kept clean (Van der Meulen 1988). Although the Rotronic MP-100 sensor has been used with relative success to measure moisture in the marine boundary layer, recent results in one case have indicated that this instrument may suffer from hysteresis after periods of high relative humidity (Katsaros *et al.* 1994). This problem will be discussed in greater detail in Sections 4a and 5 of this paper.

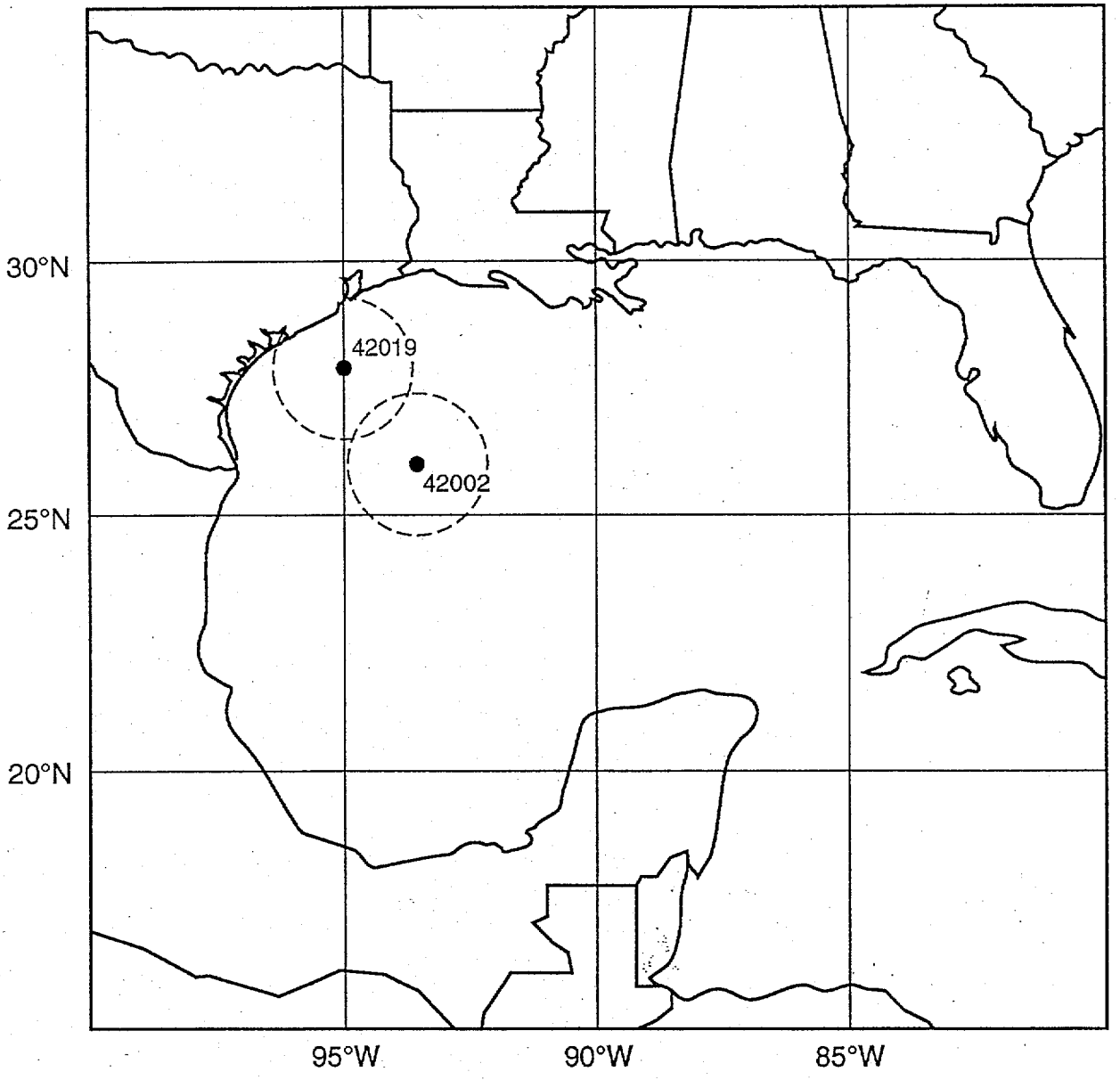

Figure 1. The locations of NDBC buoys at stations 42019 (27.9N, 95.0W) and 42002 (25.9N, 93.6W) are shown together with co-located circles within which ship reports for search radii of 150 km were acquired. The distance separating the buoys is 263 km.

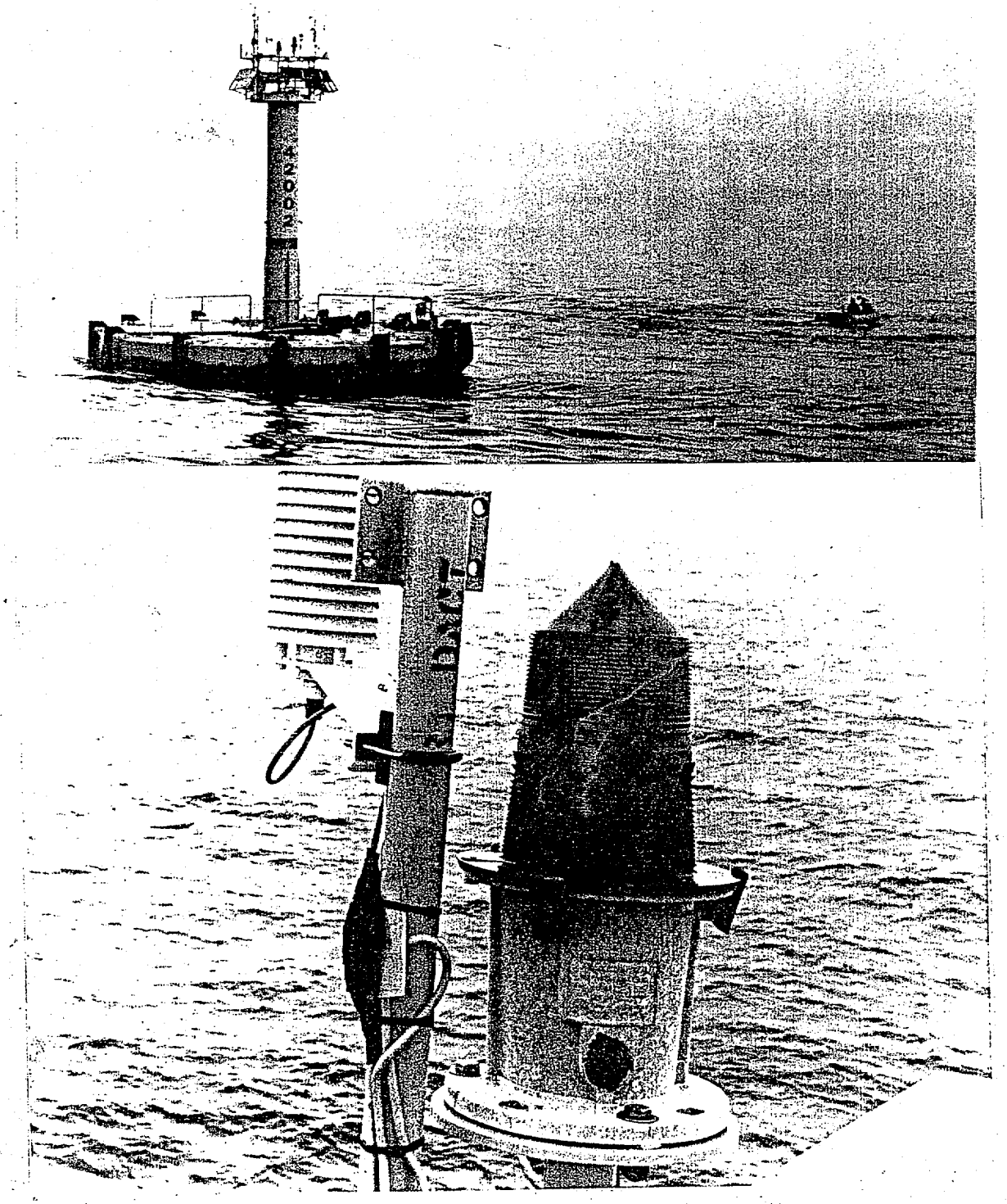

Figure 2. The top panel (2a) shows a photograph of the 10 meter discus buoy moored at 42002. Note the small boat to the right for comparison. The lower panel (2b) shows the Rotronic sensor mounted on this buoy. This instrument is located at a height of 10 meters above the water line.

b. Deployment

Rotronic humidity sensors were installed on two NDBC buoys in the Gulf of Mexico located at 27.9N, 95.0W (station number 42019) and at 25.9N, 93.6W (station number 42002) (Fig. 1). The bottom depth at station 42019 is approximately 120 m, and at station 42002 it is approximately 3200 m. The sensor on 42019 was installed on 4 May 1993; the sensor on 42002 was installed on 4 June 1993. A six-meter NOMAD platform is at 42019 and the Rotronic sensor was located at a height of 5 meters above the water line. There is a 10-meter discus buoy at 42002 and the Rotronic sensor in this case was located at a height of 10 meters above the water line. Figure 2 shows the discus buoy moored at 42002 (Fig.2a) and the Rotronic sensor which was mounted on this platform (Fig.2b).

c. Calibration

Figure 3 shows pre- and post-calibration data for the instrument installed at station 42019. This sensor was calibrated on 27 January 1993 prior to its deployment on 42019 and functioned normally until it was retrieved on 25 January 1994. The Rotronic sensor at station 42002 has been operating continuously since its original deployment. When the sensor at 42019 was recalibrated on 24 March 1994, there was a calibration shift of less than 2%. Most of this shift occurred at relative humidities of 70% or less. Finally, both the pre- and post-calibrations for 42019 agreed with the reference values within the WMO accuracy standards (shown by the dashed lines in Fig. 3) which require accuracies of ±5% for relative humidities of up to 50%, and ±2% for relative humidities above 50% (WMO 1983).

d. Reliability

Since the Rotronic sensors were first installed on NDBC buoys along the West Coast, their reliability has steadily improved. Figure 4 shows the percentage of instruments that survived more than six months as a function of the year the sensor was deployed. This percentage increased from 18% in 1990 to 60% between 1992 and 1994 because of improved cabling and calibration. The mean time between failures for sensors deployed since 1991 is eight months with one sensor lasting 15 months. Figure 5 examines these percentages based on buoy hull type. The humidity sensors are located five meters above the water line on the three-meter discus (3D) and the six-meter NOMAD (6N) buoys. On the 10-meter discus (10D) buoys, the sensors are located 10 meters above the water line. The survival percentages on the small buoys are almost identical to those on the larger 10D buoys even though senor contamination from salt spray is most likely greater on the 3D and the 6N buoys. This survival pattern has not changed with time and is significant because most of the new buoys that are being deployed by NDBC are either the 3D or the 6N hull types.

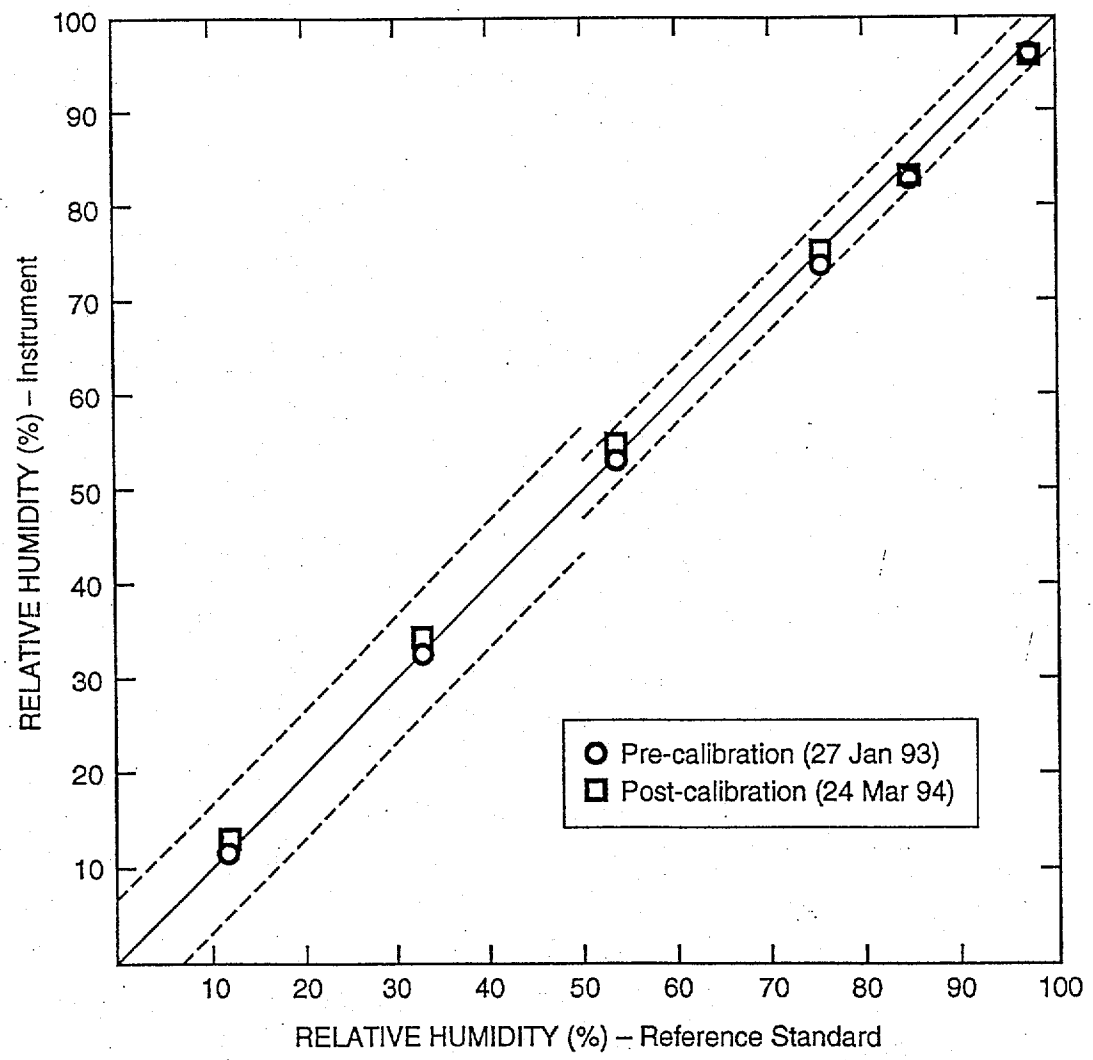

Figure 3. Pre- and post-calibration data for the Rotronic humidity sensor installed on the buoy at station 42019 between 4 May 1993 and 25 January 1994. The dashed lines indicate the accuracy limits established by the WMO for humidity sensors. Both pre- and post-calibrations fall well within the specified limits.

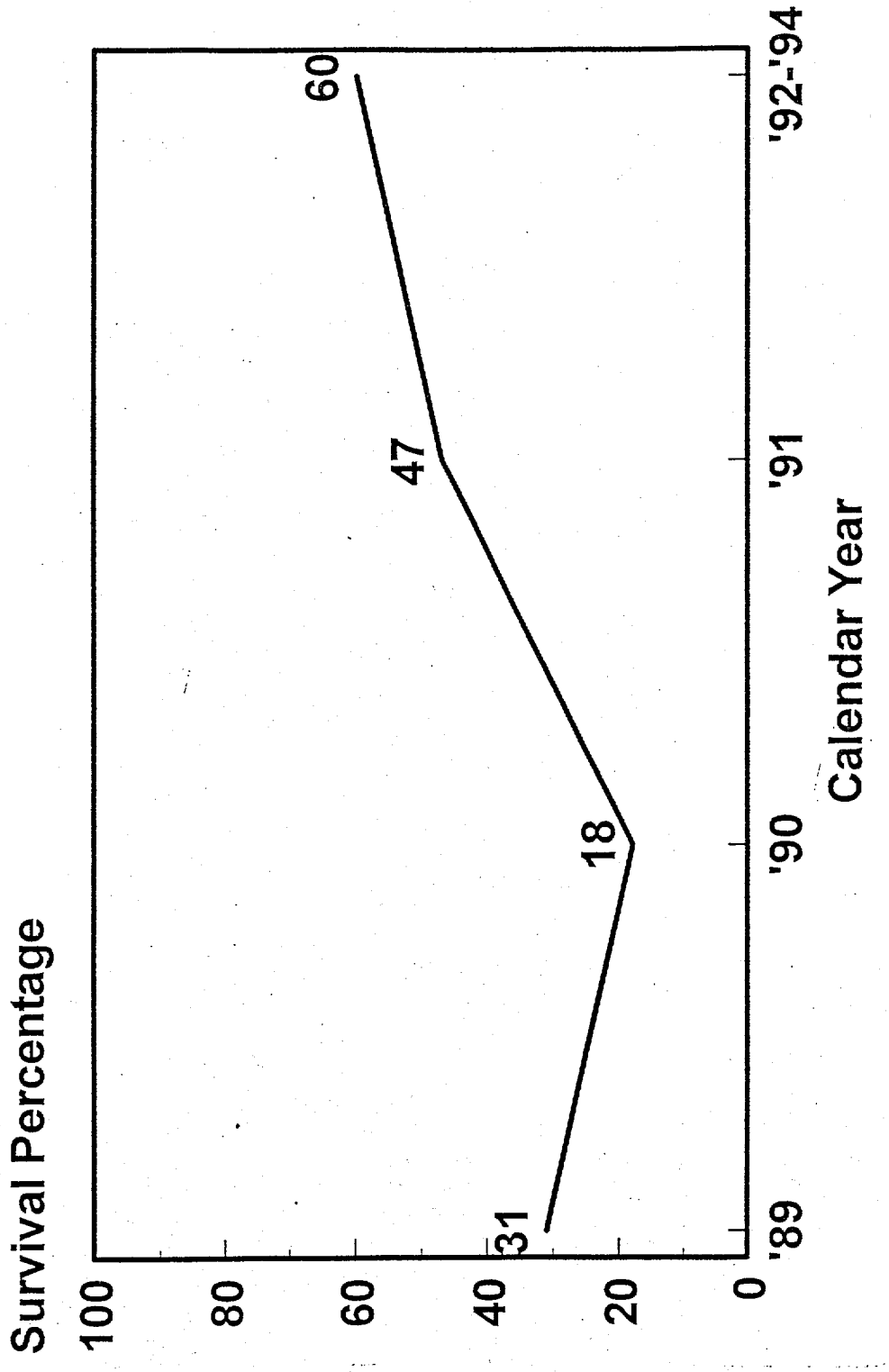

Figure 4. Reliability for the Rotronic sensors deployed on various NDBC buoys is indicated by the percentage of instruments that survived for more than 6 months as a function of the year when the sensor was deployed. See text for additional information.

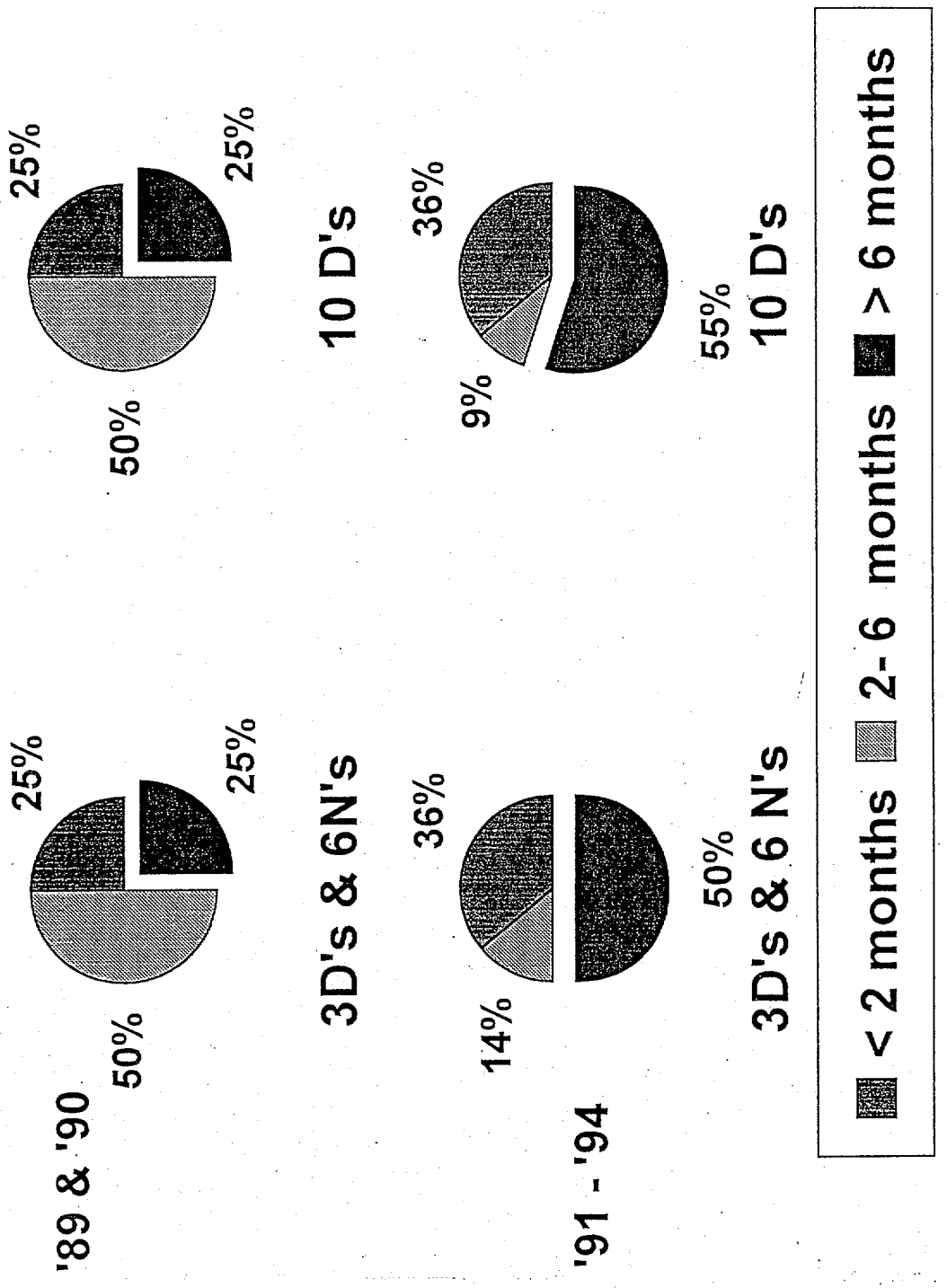

Figure 5. Survival percentages as a function of hull type. Note that the survival percentages for the smaller 3D and 6N buoy hull types are almost the same as for the larger 10D buoy hull type.

3. DATA ACQUISITION AND ANALYSIS

a. Acquisition

The following environmental parameters were acquired from the buoys at stations 42019 and 42002: barometric pressure, eight-minute average wind speed and direction, air temperature, sea surface temperature, relative humidity, and wave spectra. The winds at 42019 were acquired at an elevation of 5 meters above the surface while the winds at 42002 were acquired at an elevation of 10 meters above the surface. Dew point temperature was also provided with these data, but this parameter is not measured directly; rather, it is calculated from the relative humidity, the air temperature and the barometric pressure. The observations were acquired hourly and extend from 00Z, 5 June to 23Z, 30 November 1993, spanning a period of nearly 6 months. Less than 0.5% of the data did not meet NDBC's standards for quality control[1], or were missing. In these cases, previous values were either repeated or linear interpolation was used to fill in the missing data or to replace erroneous data in order to complete the time series. Sea surface temperature is measured through the hull at a depth of one meter by a thermistor insulated from the interior hull environment.

b. Moisture and flux calculations

Specific humidities were calculated according to Gill (1982) where the specific humidity of the air is given by

$$q_a = (0.62197 e_a) / (P - 0.378 e_a)$$

and the specific humidity at the ocean surface is given by

$$q_s = (0.62197 e_s) / (P - 0.378 e_s)$$

assuming that the air is saturated at the surface. q_a and q_s are expressed in grams of water vapor per gram of moist air. e_a represents the vapor pressure of air (hPa), e_s the saturation vapor pressure (hPa) at the temperature of the ocean surface, and P is the barometric pressure (hPa) at sea level.

e_a and e_s are in turn calculated according to

$$e_a = RH e_s / 100.0$$

---

[1]Quality control of humidity data at NDBC includes automatic flagging of the data for which the relative humidity (RH) is <0% or >102%, and a time continuity check for which the change in RH must be ≤25% per hour. Temperature-dew point inversions are also flagged. Finally, all flags which are raised automatically are checked manually (T. Mettlach, personal communication).

where RH is the relative humidity in percent, e_s is given as

$$e_s = Kx10^{v}[1.0 + 1.0x10^{-6}P(4.5 + 0.0006T_s^2)]$$

T_s is the sea surface temperature (° C), v is computed from

$$v = (0.7859 + 0.03477T_s) / (1.0 + 0.00412T_s)$$

and K is a reduction factor for saturation vapor pressure over seawater. At a salinity of 35 ppt (assumed here), K is taken to be 0.98 (Kraus 1972).

In order to calculate the fluxes of sensible and latent heat, the wind speeds at both buoys were adjusted to a common reference height of 10 meters. Since the winds at 42002 were initially acquired at a height of 10 meters, no adjustment was required in this case. For the winds at 42019, however, an adjustment based on a logarithmic wind speed profile relation was employed which assumes conditions of neutral or near-neutral stability (Roll 1965).

Surface heat fluxes were calculated from the appropriate buoy observations and the specific humidities according to the bulk aerodynamic formulas of Friehe and Schmitt (1976) for sensible heat flux and according to Gill (1982) for latent heat flux. The sensible heat fluxes were calculated according to three conditional formulas for stability. In each case, the product $U\Delta T$ of the wind speed at 10 meters (U) and the difference in temperature (ΔT) between the sea surface temperature (T_s) and the air temperature at 10 meters (T_a) is required. For quasi-neutral to near unstable conditions, with $0 < U\Delta T < 25$ (m°K/sec), the sensible heat flux (Q_s in W/m^2) is given by

$$Q_s = \rho C_p(0.002 + 0.00097U\Delta T)$$

where ρ is the density of air (1.235 kg/m^3), and C_p is the specific heat of air at constant pressure taken as equal to $1004.6(1.0 + 0.8375q_s)$ in Joules/kg/°K (Gill 1982). For stable conditions, $U\Delta T < 0$, Q_s is given by

$$Q_s = \rho C_p(0.0026 + 0.000864U\Delta T)$$

For unstable conditions, $U\Delta T > 25$, Q_s is given as

$$Q_s = \rho C_p(0.00146U\Delta T)$$

The latent heat flux was calculated according to

$$Q_e = \rho C_e U L_v(q_s - q_a)$$

where C_e is a dimensionless coefficient taken to be 1.5×10^{-3}, L_v is the latent heat of vaporization taken to be $2.5008 \times 10^6 - 2.3 \times 10^3 T_s$ in Joules/kg, and ρ, U, q_s, q_a, and T_s are the same.

Finally, the Bowen ratio was calculated by taking the ratio of the sensible heat flux (Q_s) to the latent heat flux (Q_e).

c. Wave calculations

Vertical acceleration at the buoys is measured every 0.67 seconds for a period of 20 minutes each hour. The acceleration records are integrated and Fourier-transformed to obtain the wave energy density spectrum. Wave energy density spectra (F(f)) were calculated with a resolution of 0.01Hz for frequency ranges of 0.03-0.4Hz and 0.03-0.5Hz at 42002 and 42019, respectively. From these spectra, three additional wave parameters have been calculated. The first is the significant wave height H_s, defined as

$$H_s = 4.0 \sqrt{\int_0^\infty F(f) dF}$$

which provides a direct measure of the wave activity.

Since we are primarily interested in the wave parameters which may be related to the exchange of moisture between the ocean and the lower atmosphere, the process of wave breaking immediately comes to mind. However, wave breaking is a discrete process in time, which is not directly captured in the above frequency-domain representation of the wave observations. The intensity of wave breaking, however, appears to be related to the development stage of the wave field, which also governs wave-induced surface roughness. The latter parameter is thus also linked directly to the surface moisture flux and is a parameter which can be estimated directly from the wave energy density spectrum. The overall development stage of the wave field can be described with the inverse wave age ε,

$$\varepsilon = U/C$$

where C is the phase velocity corresponding to the peak frequency of the spectrum, and U is the wind speed. The peak frequency, f_p, is estimated from the maximum discrete energy density and its neighboring values by fitting a second-order polynomial to the spectra. From this frequency, C is determined using the standard dispersion relation for wave speed for a water body of arbitrary depth. $\varepsilon = 1$ corresponds to a fully-developed

wind sea, i.e., a wind sea in equilibrium with the local wind sea, $\varepsilon > 1$ corresponds to growing wind waves and $\varepsilon < 1$ corresponds to swell. The wave-induced contribution to the surface stress is important for young waves only ($\varepsilon > 1$).

Because the wave-induced roughness is primarily related to high-frequency wave energy, another parameter of interest is the nondimensional energy of the high-frequency flank of the spectrum α, also known as the 'Phillips' constant (Phillips 1958), where

$$\alpha = (2\pi)^4 / g^2 (f_h - f_1) \int_f^{f_h} F(f) f^5 df$$

and

$$f_1 = 1.5 * \max(f_p, f_{PM})$$

$$f_h = \max (2.5*f_p, 2.5*f_{PM}, f_{max})$$

f_{PM} is the Pierson-Moskowitz frequency (Pierson and Moskowitz 1964) which is the frequency for which $\varepsilon = 1$ for a given wind speed, and f_{max} is the highest spectral frequency observed. α, is a measure of the small-scale roughness of the ocean surface, and, therefore, of the wave-induced surface stress. For a fully-developed sea, $\alpha \approx 0.01$, and the wave-induced stress again will be small. For larger α, active wave growth occurs, and waves will contribute significantly to the surface stress. For smaller α, the contribution of waves to the surface stress is small. In such cases most of the wave energy can be attributed to swell. The limited range of frequencies for which the wave autospectra are observed however, makes it impossible to evaluate α for low wind speeds and/or low wave heights. This parameter has only been evaluated for cases where the integral encompasses at least four discrete spectral densities. Note that α is still an indirect measure of the surface roughness, since the actual roughness is primarily related to near-capillary waves, well outside the range of the present wave observations. Furthermore, ε and α generally behave similarly, since they can be considered as large-scale (ε) or small-scale (α) estimates of the wave-induced surface roughness.

4. RESULTS

a. Validation

To provide a measure of validation for the observations of moisture acquired from the buoy-mounted Rotronic humidity sensors, we have produced matchups of buoy data with measurements of boundary layer moisture acquired from selected ships and fixed platforms (primarily oil rigs) in the surrounding area. The majority of ship reports came from two NOAA research vessels (NOAA Ships OREGON II and CHAPMAN) which were at sea

in the Gulf of Mexico during the study period. Each vessel was equipped with wet and dry bulb thermometers and used standard WMO data collection and reporting procedures.

All of the reported moisture values obtained from the ships and fixed platforms were converted to specific humidities for direct comparison with the calculated specific humidities from the buoys. The observations from each source were matched to within one hour in time and were made over a range of search radii from each of the buoys. The search radii were increased in 25 km steps from 50 out to 300 km for each buoy. The choice of search radii was based on:

- (1) an e-folding correlation distance for specific humidity of ~ 800 km in the northern Gulf of Mexico(see the following subsection for details), and
- (2) the need for adequate sample sizes.

Figure 1 shows matchup circles for each buoy with search radii of 150 km. Scatter plots for matchups within a search radius of 175 km of each buoy are shown in Fig. 6. Biases, RMS differences, and correlations between the buoys and the ship reports are given in Table 1 for search radii of 50 to 300 km (in 50 km steps). The statistics become repeatable (*i.e.*, stabilize) at sample sizes of the order of 300, which correspond to search radii of 150 and 250 km for buoys 42019 and 42002, respectively. Although the buoy moistures on average tend to be slightly higher than the ship reports for the sensor on 42019 (indicated by the positive biases), the opposite is true for the sensor on buoy 42002. The RMS differences are slightly higher and the correlations lower for the sensor on buoy 42002. Overall, the correlations between the buoys and the ship reports are high; thus, these comparisons are generally favorable. However, a more conclusive validation study would have required comparisons with reference standards located side-by-side with the Rotronic sensors on each buoy.

Katsaros *et al.* (1994) recently conducted field tests of a number of humidity sensors including the Rotronic MP-100 instrument. Hysteresis was found to occur for mean humidities following high-moisture events for the Rotronic MP-100 instrument. The greatest differences between the Rotronic sensor and a reference psychrometer occurred at relative humidities less than 70%, particularly after periods of high relative humidity. The Rotronic sensor apparently required time to dry out after periods of high moisture. Finally, a bias of 8% between the Rotronic MP-100 and a reference psychrometer was not due simply to a calibraton error but was attributed in part to hysteresis by the sensor.

To address the problem raised by Kataros et al., we first looked for periods of high relative humidity in our data. Cumulative distributions of relative humidity for each buoy indicate that only about 8% of the data from either buoy have relative humidities that exceed 90%, and only about 2% of the data exceed 95%. Overall, very few periods of identifiable rain occurred during the study period and those periods which could be identified did not coincide precisely with any of our ship reports. To examine the

hysteresis problem adequately with our data would have required locating matchups that occurred within a narrow window of several hours following clearly-defined high-moisture (*i.e.*, saturation) events and, as indicated, no such matchups were found. Our comparisons with the ship reports above, however, showed only small biases (3.6% for 42019 and -4.1% for 42002). If hysteresis was a serious problem, we would have expected both biases to be positive (*i.e.*, buoys to be higher than the ship reports). This result, of course, was also influenced by the fact that high relative humidities (>~95%) were a relatively rare occurrence in our data. In summary, our data are not adequate to address the hysteresis problem raised by Katsaros et al. However, based on the limited data available, no evidence for a significant hysteresis problem could be found for the Rotronic sensors deployed on buoys 42019 and 42002. Also, based on the results of Visscher and Schurer (1985), Muller and Beekman (1987), and Hundermark (1989), hysteresis problems were not previously found with the Rotronic MP-100 instrument.

Table 1. Comparisons of specific humidities at NDBC buoys 42019 and 42002 with those computed from nearby ship and fixed platform observations at various radii from each buoy.

Range (km)	Sample Size	Bias	RMS	Correlation Coefficient
Station 42019				
50	49	0.00043	0.00133	0.932
100	170	0.00059	0.00166	0.893
150	326	0.00089	0.00200	0.868
200	472	0.00081	0.00204	0.867
250	622	0.00073	0.00200	0.867
300	733	0.00067	0.00202	0.852
Station 42002				
50	8	-0.00167	0.00220	0.780
100	33	-0.00132	0.00223	0.550
150	101	-0.00146	0.00276	0.712
200	166	-0.00098	0.00237	0.728
250	333	-0.00084	0.00214	0.786
300	580	-0.00071	0.00224	0.780

b. Interpretation of the synoptic-scale variability

The variability of moisture within the marine boundary layer at buoys 42019 and 42002 occurred on several time scales; however, the synoptic-scale variations in moisture stand out as the dominant source of variability, particularly during September, October and November (Fig. 7). In order to examine this synoptic-scale activity in greater detail, we studied the appropriate surface weather maps.

On 17 June 1993, specific humidity decreased, and the surface heat fluxes increased at both buoys, reflecting the influence of a tropical wave that formed near the Yucatan Peninsula. Specific humidities remained relatively low for about 4 days, during which time the tropical wave intensified becoming first a tropical depression and then Tropical Storm Arlene. Arlene moved to the NNW across the Gulf, approaching the buoys from the south. Arlene followed a path that took it west of buoy 42002, producing stronger responses in terms of moisture and heat flux at 42002 than at 42019. The decrease in specific humidity at the surface conincided with decreases in SST of ~2C, which were most likely produced by mixing in the oceanic surface layer.

On 26 September, specific humidity dropped suddenly at both buoys due to the first significant cold front of the fall season. This system was composed of two fronts, a weaker cool front closely followed by a more intense cold front. On 27 September, the first front weakened significantly, while the second front passed the buoy at 42019 on its way toward 42002. Later on the 27th, the dominant front passed 42002 with increasing wind speeds and falling air and dew point temperatures. Dew point temperatures dropped by over 10C at 42019 and by ~5C at 42002, indicating that the air mass behind the front was not only cold, but relatively dry. The impact of this frontal passage was clearly greater at 42019 than it was at 42002 for all buoy parameters. By 30 September, the impact of the front had practically disappeared at both buoy locations. Moisture, in particular, was greatly affected by the passage of this frontal system and, as a result, served as an excellent indicator of frontal behavior.

Starting on 21 October, a series of cold fronts began dropping down into the Gulf of Mexico and continued with some regularity through the end of November. Between 21 and 29 October, two cold fronts entered the Gulf from the NW and within a day or two each system had weakened sigificantly. On 30 October, a rapidly-moving, intense frontal system entered the Gulf from the north. The air mass behind this front was extremely cold and dry. Dew point temperatures at 42019 dropped to a low of 3.9C and at 42002 they reached 6.7C as the center of high pressure behind the front continued to move south and into the area where the buoys were located. Fig. 8 shows the surface analysis for 18Z on 30 October from NMC's Aviation Model. This analysis clearly depicts the intensity of this frontal system at one point in its progression across the Gulf although it lags the buoy observations by almost 12 hours and shows less drying behind the front (~80% observed vs. 90% from the analysis at 42019, and ~75% observed vs. 90% at 42002). It took almost

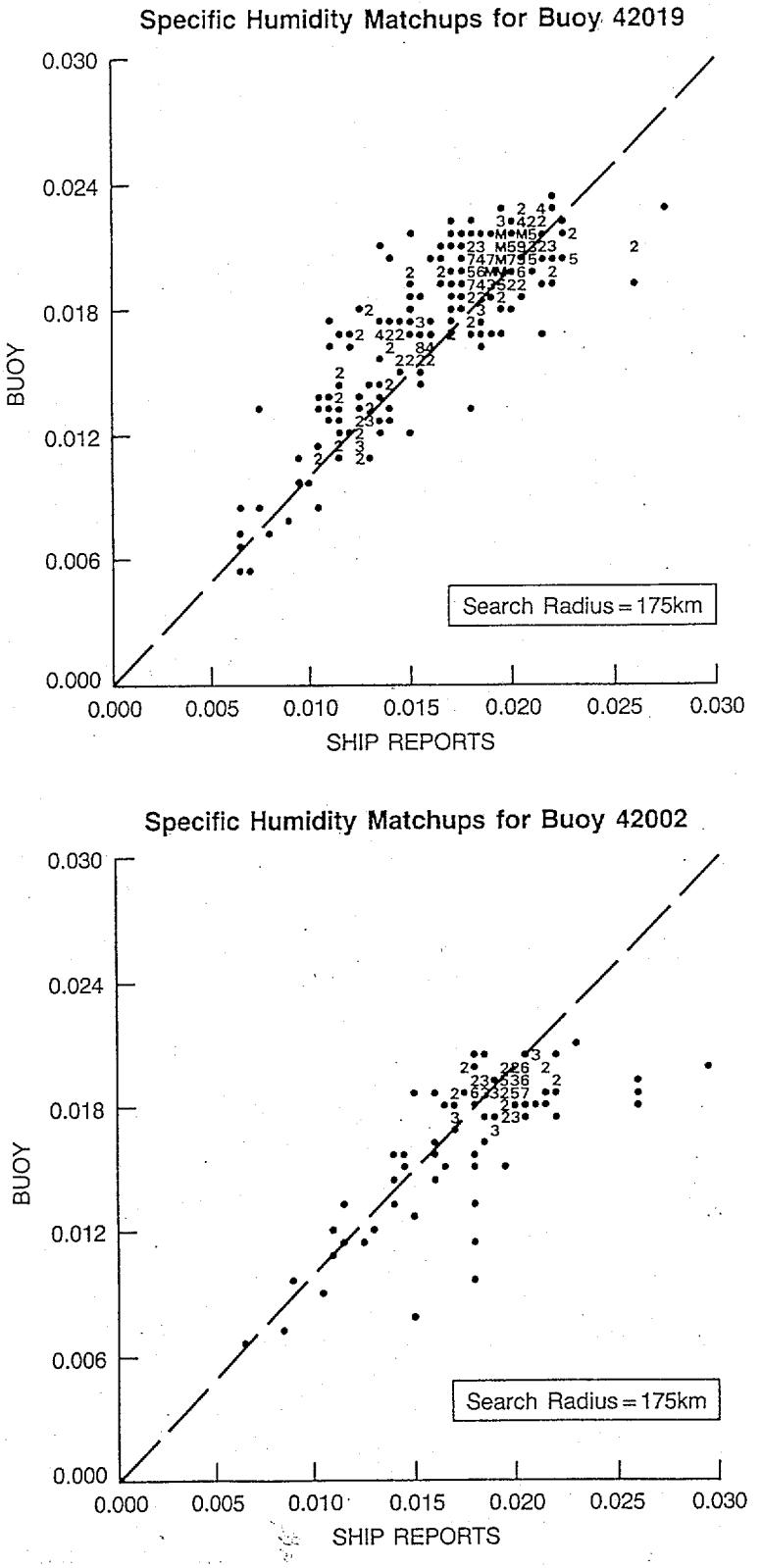

Figure 6. Scatter plots comparing specific humidities from each buoy with specific humidities reported by nearby ships located within 175 km of each buoy. Numbers in the scatter plots indicate the number of times that repeated matchup values of specific humidity occured.

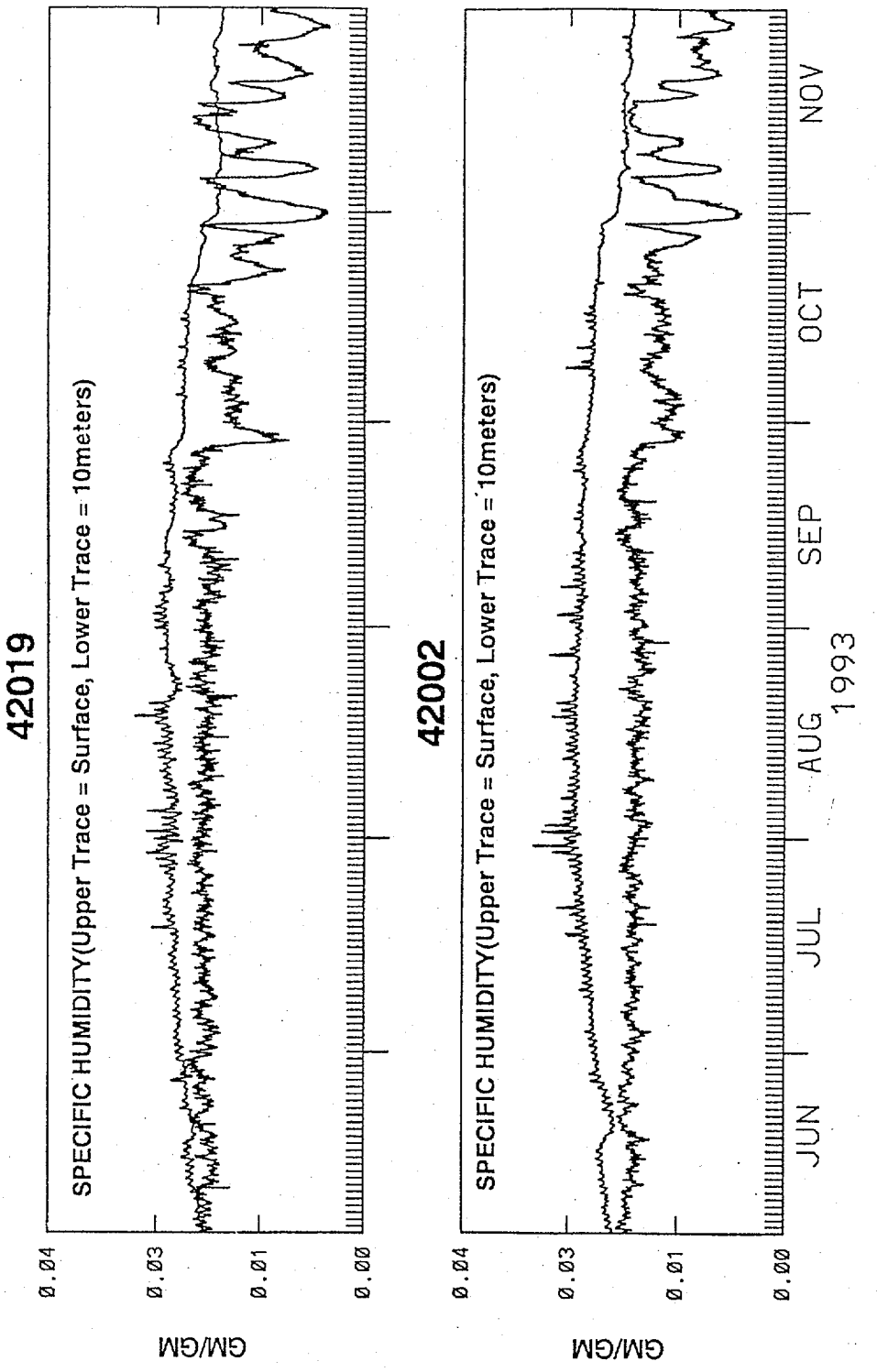

Figure 7. The time series of specific humidity at the surface and at 10 meters for the period 5 June through 30 November 1993 are plotted in the upper panel for 42019 and in the lower panel for 42002. In each case, the upper trace represents specific humidity at the surface.

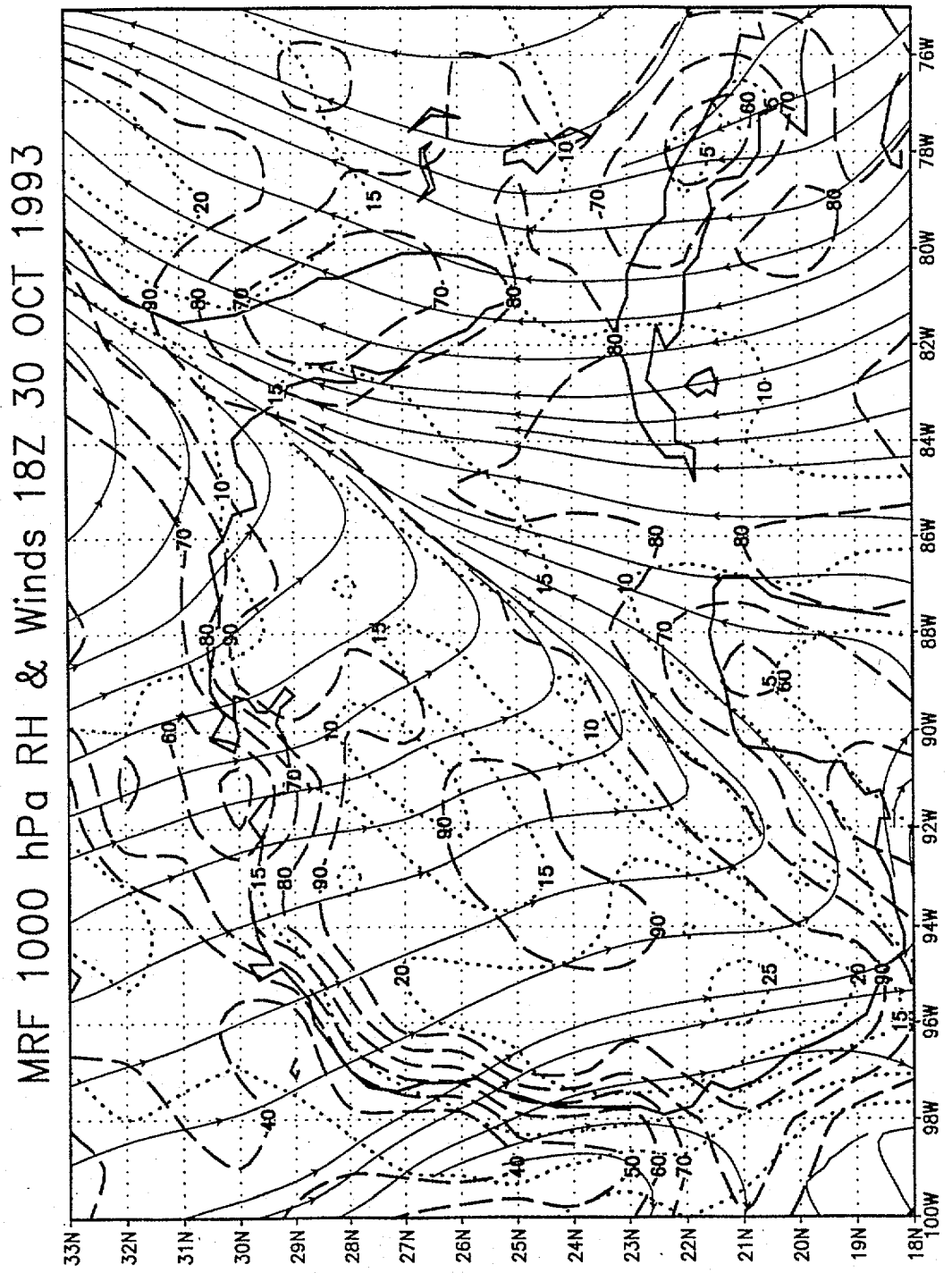

Figure 8. Surface analysis from NCEP's Global Spectral Model for 18Z on 30 October 1993. Streamlines (solid contours) and isotachs [dotted contours (knots)] represent the winds, and the heavy dashed lines represent contours of relative humidity.

5 days for pre-frontal conditions to be re-established over the Gulf following the passage of this frontal system. On 6 November, another cold front dropped down into the northern Gulf close behind the previous front. Although this frontal system was intense, it was slightly weaker than the previous system.

Between 9 and 11 November, a small high-pressure system dropped down over the northern Gulf bringing slightly cooler and drier continental air with it, unlike the previous events which were primarily frontal in nature. Between 17 and 30 November, three more cold fronts dropped down into the Gulf of Mexico causing air and dew-point temperatures to drop significantly at the two buoy locations.

In summary, the events described above produced strong and well-defined signatures in the moisture-related observations, emphasizing the importance of these data in characterizing synoptic-scale variability in the near-surface marine environment.

c. Time series of environmental parameters

Time series of sea-level pressure, wind speed, wind direction, sea surface temperature, air temperature, dew point temperature, relative humidity, and wave height for each buoy are shown in Figs. 9 (42019) and 10 (42002). All parameters were acquired directly from sensors on the buoys except for dew point temperature which was calculated from the relative humidity, air temperature and barometric (sea-level) pressure.

By the second week in September, greater variability occurs in pressure, wind speed and wind direction. By late September and particularly by late October, much greater synoptic-scale variability occurs for air temperature and the moisture-related parameters. These increases in variability are clearly related to the seasonal change to fall conditions when frontal systems from the continental U.S. begin dropping as far south as the Gulf of Mexico.

Figure 7 shows the time series of specific humidity at the surface and at 10 meters for stations 42019 (upper panel) and 42002 (lower panel). Specific humidity at the surface follows sea surface temperature, upon which it is primarily based, not responding strongly to the atmospheric conditions above, at least on synoptic and shorter time scales. As a result, the pattern of variability which occurs at the surface is quite different from that which occurs at 10 meters. Surface specific humidity in most cases exceeds that at 10 meters. However, during brief periods in October and November, the specific humidity at 10 meters exceeds that at the surface (for buoy 42019 only). These reversals occur during periods of rapid change or recovery from the passage of cold, dry frontal systems and prior to the return of equilibrium conditions within the marine boundary layer. Overall, these time series reveal three scales of variability, small-scale (of the order of hours), synoptic-scale (of the order of several days), and seasonal (several months). The greatest variability is clearly associated with the synoptic-scale events.

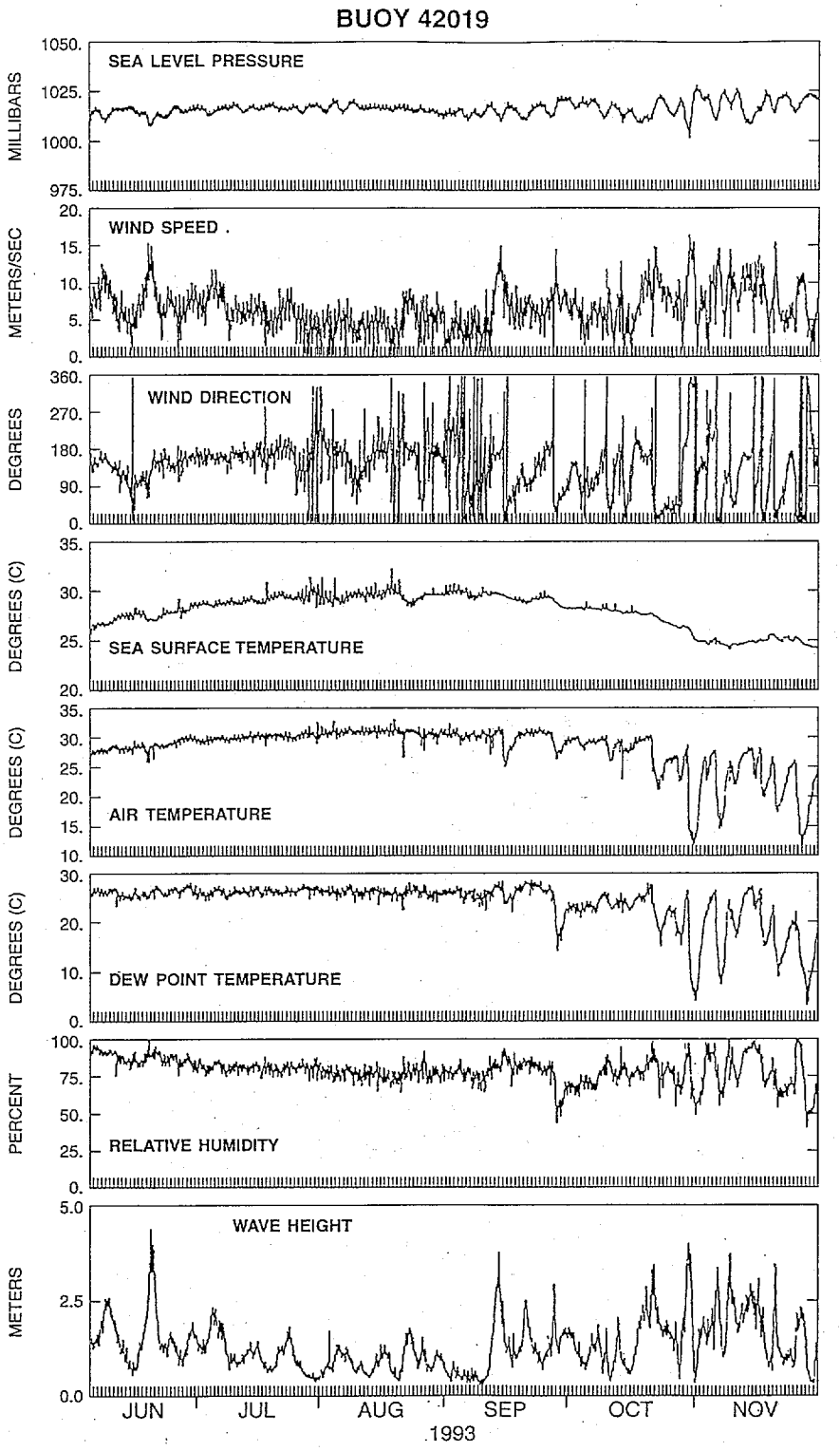

Figure 9. Time series of hourly sea-level pressure, wind speed, wind direction, sea surface temperature, air temperature, dew point temperature, relative humidity and wave height are shown for the period 5 June through 30 November 1993, for the buoy at station 42019.

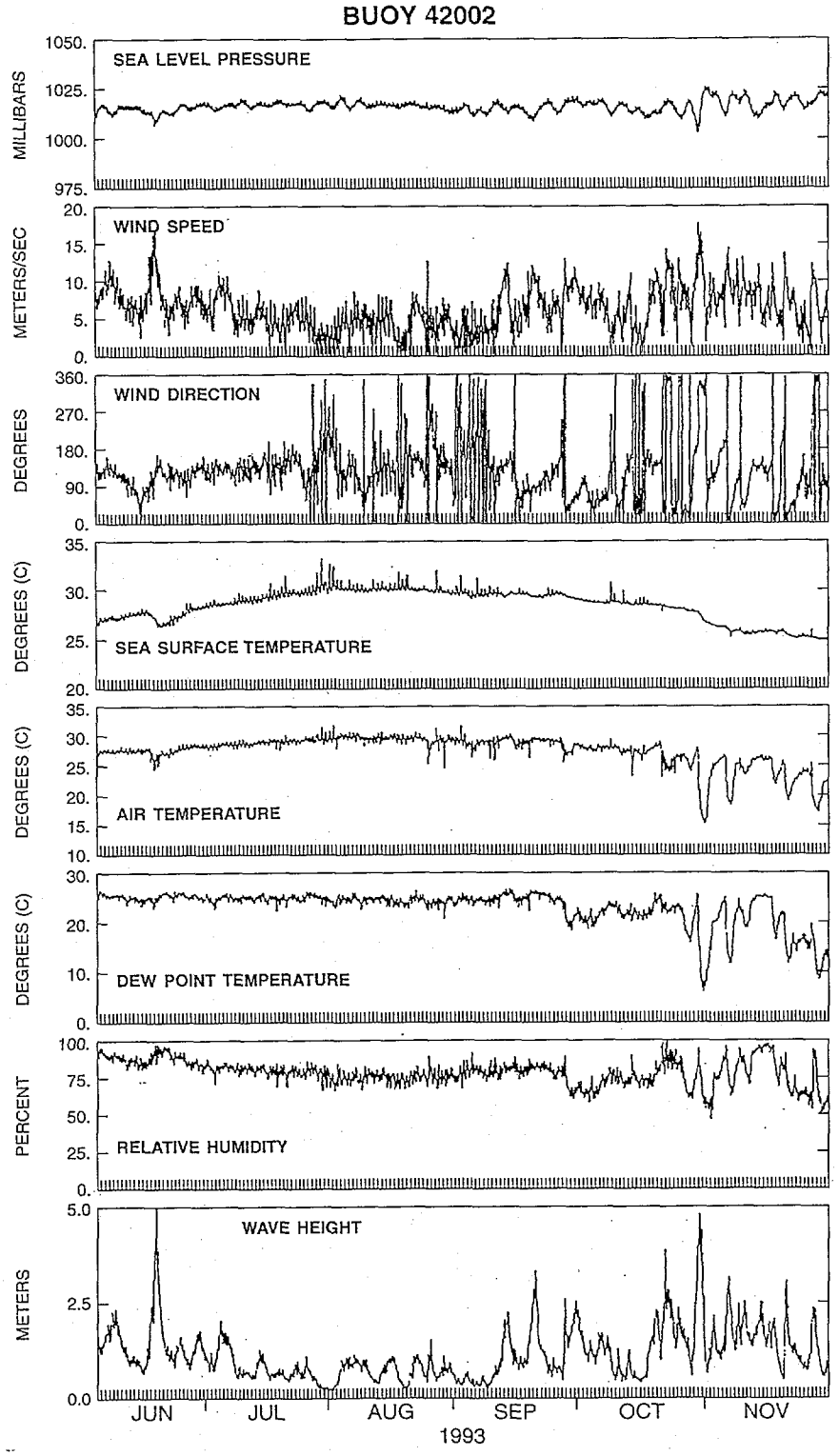

Figure 10. Same as Fig. 9 except for 42002.

Although not shown explicitly, the specific humidity time series for both buoys at the surface and at 10 meters are, at least qualitatively, very similar. Quantitative comparisons of similarity are made in the following cross-correlation analyses.

1) Cross-correlation analyses

Cross-correlation analyses were performed for the two buoy time series of specific humidity, wind speed, barometric pressure, air temperature, wave height and sea surface temperature. The maximum cross-correlations and the corresponding lags are presented in Table 2. The correlation coefficients consistently exceed 0.9, except for wind speed and wave height where local (wind speed) or cumulative (wave height) effects become more important. Of particular interest are the lag relationships between the time series for each parameter. Of the atmospheric parameters, air temperature and specific humidity both attain their maximum correlations at lags of -6 and -7 hours, repectively, whereas the other parameters (except for wave height) are maximally correlated at, or near, zero lag. Lags of -6 or -7 hours indicate that coherent sources of variation occur at 42019 prior to their occurrence at 42002, consistent with atmospheric disturbances which propagate from the NW (actually, most of the synoptic events examined tended to enter the Gulf from the north rather than the NW, so we are only able to resolve a component of the true direction) with speeds on the order of 40-50 km/hr. Only air temperature and moisture, of the parameters examined, appear to serve as reliable tracers of the motion. Based on a maximum cross-correlation of 0.91 for specific humidity, a separation distance of 263 km between the buoys, and an exponential decay law, the e-folding distance for this parameter is approximately 850 km, indicating that variations in moisture are spatially coherent over relatively large distances in the northern Gulf of Mexico. With respect to wave height, a

Table 2. Cross-correlation statistics for the entire series of hourly values for the environmental parameters included below from 0000 UTC, 5 June to 2300 UTC 30 November 1993.

Environmental Parameter	Cross-correlation	Lag (hours)[1]
Specific Humidity	0.911	-7
Wind Speed	0.678	-1
Barometric Pressure	0.939	0
Air Temperature	0.943	-6
Significant Wave Height	0.820	-5
Sea Surface Temperature	0.910	0

[1]Negative sign indicates that the series at 42019 leads the series at 42002.

lag of -5 hours indicates that the prevailing direction of propagation for surface gravity waves in the northwestern Gulf of Mexico lies roughly between the southwest and northeast quadrants.

Successive cross-correlations for specific humidity were also calculated for 7-day (168-hour) periods, stepping through the data hour-by-hour. The results are displayed in Fig. 11, where both the maximum cross-correlations (upper panel) and the corresponding lags (lower panel) are shown. The maximum correlations increase abruptly around 7 September, and the lags change from mostly postive to essentially negative at this time, indicating that events prior to the first week in September generally arrived at 42002 before they arrived at 42019 and conversely thereafter. These significant changes in correlation structure for specific humidity reflect a seasonal change in synoptic weather conditions in the northern Gulf of Mexico. In particular, they imply that the prevailing weather patterns became more coherent and tended to enter the buoy domain from the North rather than from the South after the first week in September (see subsection (d) for further details).

2) Spectral calculations

The time series of wave height, wind speed, specific humidity, air temperature, SST, and barometric pressure have also been subjected to spectral analysis in order to further explore the character of the variability for the various buoy parameters. Prior to the spectral computations, each time series was normalized with respect to its mean; the resulting nondimensional series were then centered. The spectral computations were performed by first calculating raw spectral estimates using a Fast Fourier Transform and then smoothing the resulting periodograms with a Parzen spectral window (IMSL Inc. 1982). Figure 12 shows the autospectra for each of the buoy parameters (specific humidity in place of relative humidity) plotted together for 42019 (left-hand panel) and 42002 (right-hand panel).

All of the autospectra display similar negative slopes which are characteristic of most geophysical processes (the so-called "red noise" spectrum). Obvious spectral peaks occur at periods of 12 ("x"=2.73) and 24 ("x"=2.42) hours for barometric pressure, SST and air temperature (but no obvious peak in air temperature at 12 hours for 42019), and lesser peaks at 24 hours for wind speed. Weaker peaks can be detected at a period of ~80 hours ("x"=1.9) for most parameters, and most likely correspond to the passage of synoptic-scale events of atmospheric origin. At both buoy locations, the autospectra for wind speed and wave height are simliar (they actually cross at "x" = ~2.1 in each cast), reflecting the close relationship that exists between the forcing and the response for these parameters.

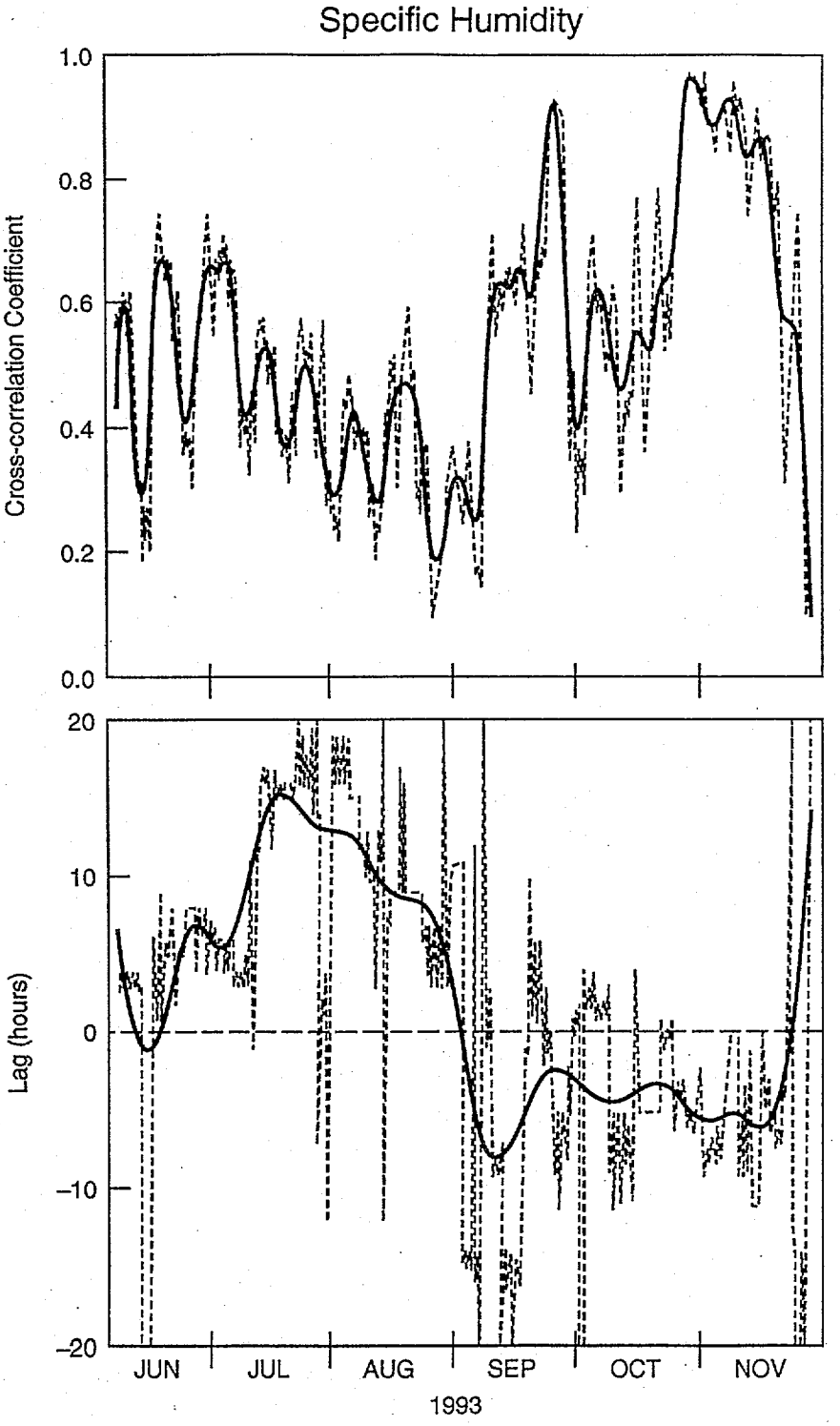

Figure 11. Cross-correlations for specific humidity between the buoys at stations 42019 and 42002 at 10 meters for successive 7-day segments of the time series at one-hour time increments. The maximum cross-correlations are plotted in the upper panel and the corresponding lags (in hours) in the lower panel. The dashed curves represent the original values and the solid curves, the results after smoothing.

d. The effects of surface gravity waves

Certain processes associated with surface gravity waves are most likely responsible for introducing moisture into the marine boundary layer. Wu (1974) has estimated that as much water enters the atmospheric surface layer through the evaporation of water droplets (from breaking waves, for example) as that which is contributed through direct evaporation from the ocean surface itself, for a wind speed of 15 m/sec at 10 m. Fairall et al. (1990) suggest that latent heat fluxes are not only related to wind speed and air-sea temperature difference, but also, at least weakly, to the surface roughness, a wave-related parameter. Based on these findings, we are motivated to examine the time series of significant wave height and several related parameters in greater detail.

Figures 13 (42019) and 14 (42002) show significant wave height, inverse wave age and the Phillips constant and latent heat flux for both buoys for the entire period. As with the other buoy parameters, several distinct weather regimes can be identified in the time histories of the various wave parameters. The first two months of record generally show quiescent wave conditions. This situation was briefly interrupted, however, by the passage of Tropical Storm Arlene from 17 to 21 June. During the first two months, the wind speed (Figs. 8 and 9) shows a well-defined diurnal cycle, which may be related to diurnal changes in the stability of the marine boundary layer (both buoys are located too far offshore to be affected by sea breeze circulations). The significant wave height shows a much smaller daily modulation since the total wave energy tends to be concentrated at the relatively low frequencies. The time scale of adjustment of waves to winds at these frequencies is relatively large, thus damping out rapid modulations of the wind speed. In contrast, high frequency wave energy has a much smaller time scale in responding to changes in the wind field, and hence is expected to show a much stronger response to the daily modulation of the wind. α does, in fact, show a large modulation, which lags the wind speed modulation by approximately 1 to 2 hours. Due to the discontinuous nature of α, this lag could not be calculated objectively, but was instead estimated by inspection. The modulation of α suggests that the surface roughness also has a large daily modulation. Because surface roughness is primarily related to wave of shorter period than those whicha re incorporated in α. Such shorter waves have an even smaller time scale of response to wind changes, and hence are expected to show a smaller time lag (if at all) with respect to the wind speed than α. The inverse wave age shows a daily oscillation similar to that of the wind speed from which it is calculated. This indicates that the peak frequency, like the significant wave height, is rather insensitive to the daily wind speed modulations.

The period covering August and the first half of September shows continued quiescent surface wave conditions, where α generally cannot be evaluated any more due to the low wind speed (and hence large f_{PM}), and/or due to the large peak frequency f of the spectrum. The wind speed and significant wave height behave as they did during the first

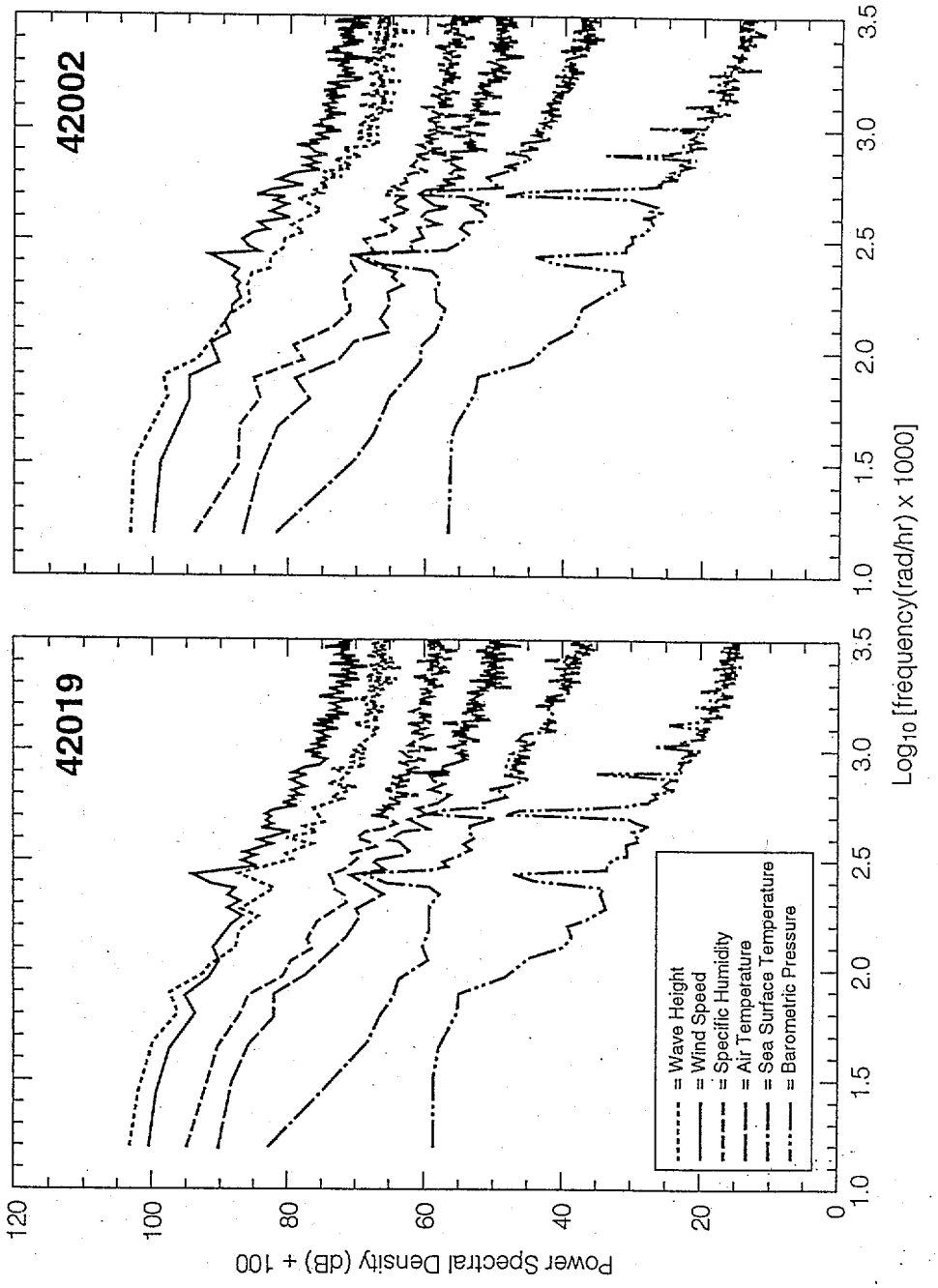

Figure 12. Autospectra for each of the buoy parameters for stations 42019 (left-hand panel and 42002 (right-hand panel). Each series was divided by its mean and then centered before the spectra were calculated. The spectra correspond to smoothed periodograms obtained by using a Fast Fourier Transform and are plotted in log-log coordinates.

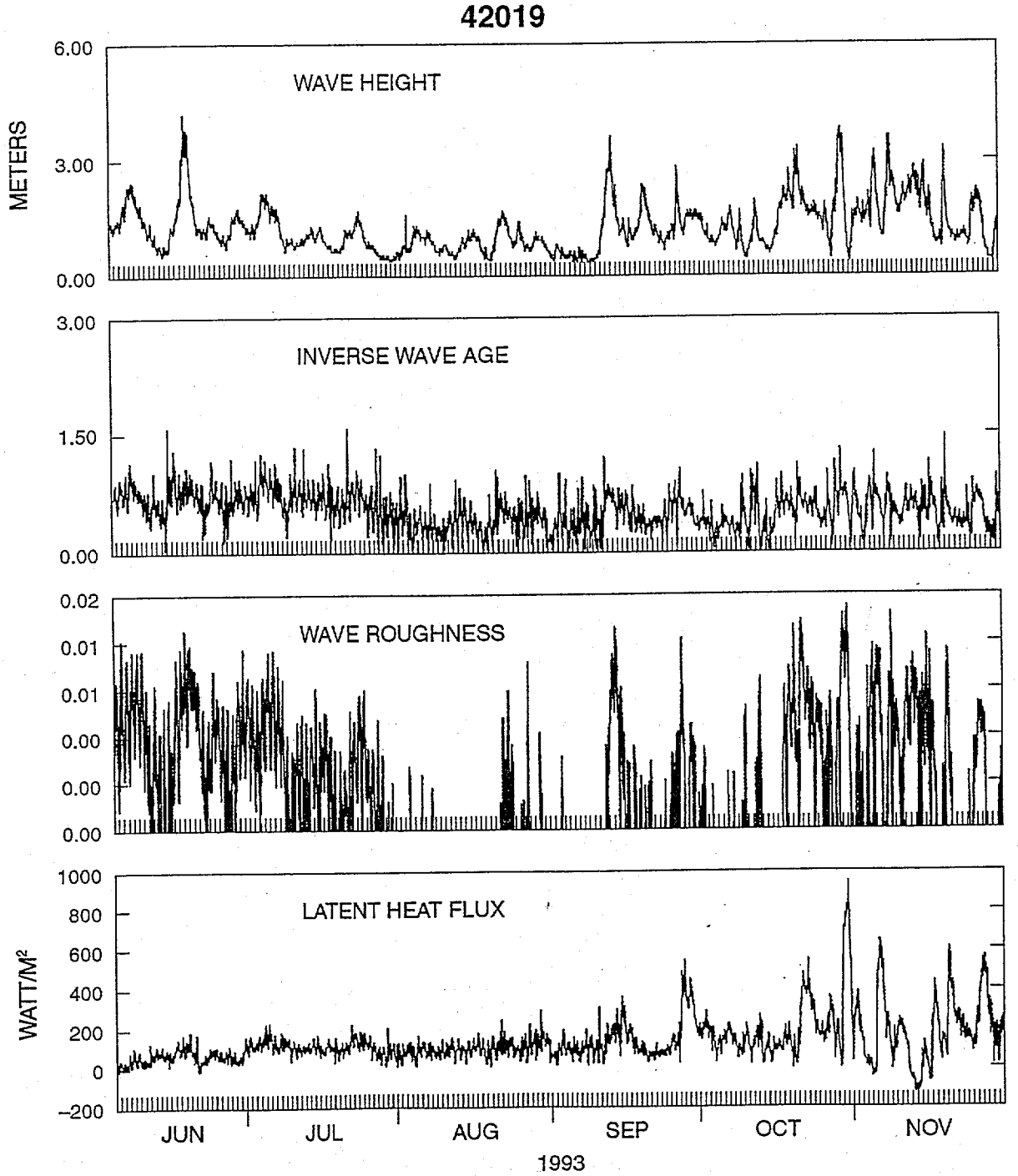

Figure 13. Time series of significant wave height, wave age (inverse), wave roughness (α), and latent heat flux for the buoy at station 42019 for the period 5 June through 30 November 1993.

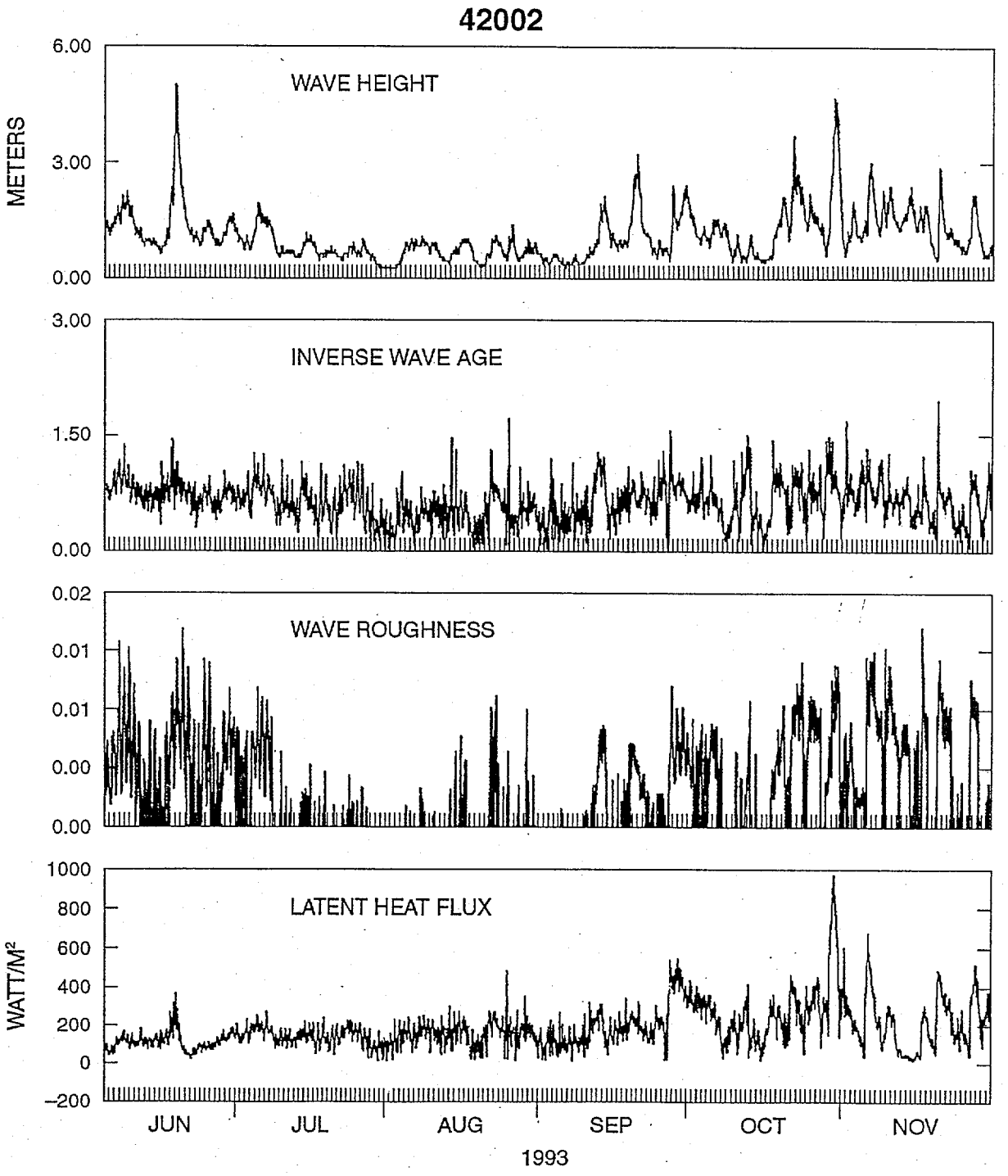

Figure 14. Same as Fig. 13 except for 42002.

two months. The inverse wave age is significantly lower than one for most of this period, indicating that the low waves are mostly comprised of swell.

As discussed earlier, the period from mid-September through the end of November shows a sequence of synoptic weather systems moving through the northern Gulf of Mexico. Particularly after mid-October at the offshore buoy (42002), the diurnal cycle in all buoy parameters either disappears, or is lost in the prevailing synoptic variability. At the near-shore buoy (42019), however, the diurnal cycle is still detectable. Several of the systems passing through the region (particularly at 42019) produce young wind seas with ϵ significantly larger than one and α significantly larger than 0.01, for which wave-induced surface roughness and wave breaking are expected to be significant. The events with the most pronounced wave-induced roughness coincide with the most pronounced heat flux events. Furthermore, all latent heat flux (LHF) events coincide with distinct wave events.

To investigate the co-occurrence of active wave growth and LHF events further, LHF is plotted as a function of α in Fig. 15. To avoid the confounding effects of the large dinurnal oscillation in α, average values for each day are presented. To ensure reasonable coverage of the daily cycle, a mini,um of 18 observations of α per day were averaged. Figure 15 indicated that the most extreme LHF events do, in fact, correspond to active wave growth conditions ($\alpha > 0.01$), in particular, at 42019. A careful comparison of he α's from the two buoy locations reveals that α is generally based on data near the limits of the frequency range that can be observed with the platforms considered. Systematic differences between the platforms might therefore be related to differences in the transfer functions for the different hull types (6 meter NOMAD at 42019 *vs.* 10 meter discus at 42002). Nevertheless, extreme LHF events clearly coincide with conditions of increased surface roughness (α) due to active wave growth. With the present observations, however, we cannot identify any functional relation between the two, but the co-occurrence of the heat-flux events and the actively growing wind seas is consistent with the production of spray and bubbles through the process of wave breaking.

In an effort to obtain additional information from these data, all wave events during the latter part of the record (plus Tropical Storm Arlene) have been examined in detail. These events contain many interesting details, but this examination also showed that each event had unique qualities, making it difficult to generalize the detailed behavior of the various wave and flux parameters.

e. Surface heat fluxes

The calculated latent and sensible heat fluxes are plotted together for buoy stations 42019 (upper panel) and buoy 42002 (lower panel) in Fig. 16. Uncertainties in these calculations are high (± several tens of W/m^2; *e.g.*, Talley 1984). Selected summary statistics for the latent and sensible heat fluxes are given in Table 3. The peak values for both fluxes correspond closely with the major synoptic events which occur between

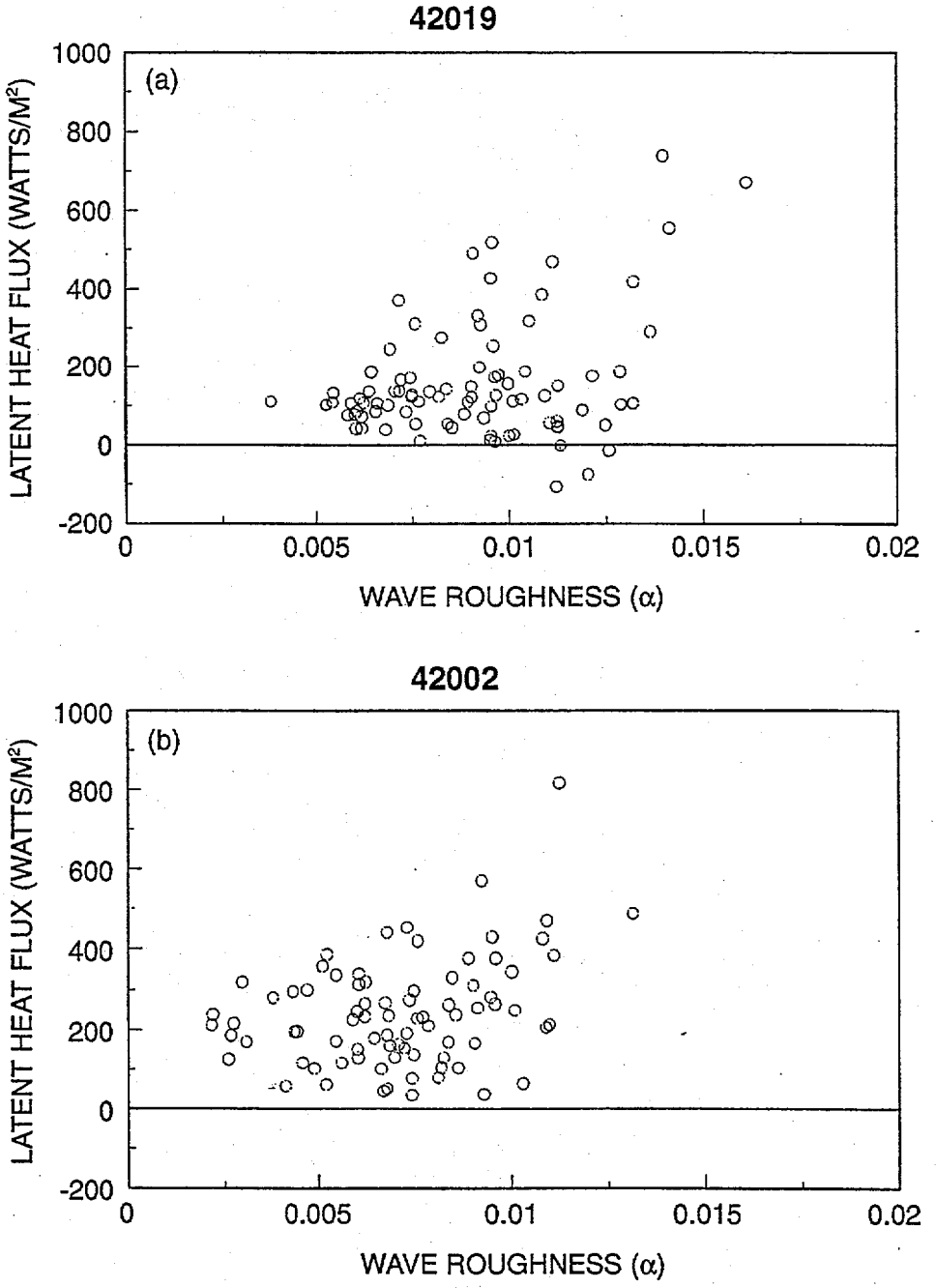

Figure 15. Latent heat flux (W/m^2) versus surface wave roughness (α) for stations 42019 (a) and 42002 (b). The data were daily-averaged before plotting which reduced the number of data points from 4296 to 179.

September and November. Upon closer inspection, the flux maxima tend to coincide with the arrival or onset of these events rather than during the subsequent periods of recovery, consistent with the occurrence of the largest near-surface (vertical) gradients of temperature and moisture, and the expected response of the marine boundary layer. Overall, the heat transfer which is primarily from the ocean to the atmosphere, is dominated by the relatively few transient events which take place after mid-September.

The latent heat fluxes far exceed the sensible heat fluxes in most cases for both buoys, consistent with similar observations made elsewhere at low latitudes (*e.g.*, Perry and Walker 1977). At 42019, the overall ratio of sensible-to-latent heat flux (*i.e.*, the Bowen ratio) was slightly greater than 6%, while at 42002, it was slightly greater than 8% (Table 3). The latent heat fluxes were almost always positive at both buoys; in contrast, the sensible heat fluxes were positive almost 100% of the time at 42002; whereas, they were only positive approximately 60% of the time at 42019, most likely reflecting the influence of lower SSTs in the nearshore region during the fall and land in relatively close proximity.

Table 3. Selected summary statistics for the Latent and sensible heat fluxes.

	42019	42002
Latent Heat Flux (LHF)		
Maximum (W/m^2)	966.3	1052.3
Minimum (W/m^2)	-135.5	3.1
Mean (W/m^2)	130.2	174.3
Time Positive (%)	97.1	100.0
Time Negative (%)	2.9	0.0
Sensible Heat Flux (SHF)		
Maximum (W/m^2)	356.0	300.3
Minimum (W/m^2)	-40.4	-7.7
Mean (W/m^2)	8.2	14.5
Time Positive (%)	60.2	97.4
Time Negative (%)	39.8	2.6
Bowen Ratio (SHF/LHF)		
	0.083	0.063

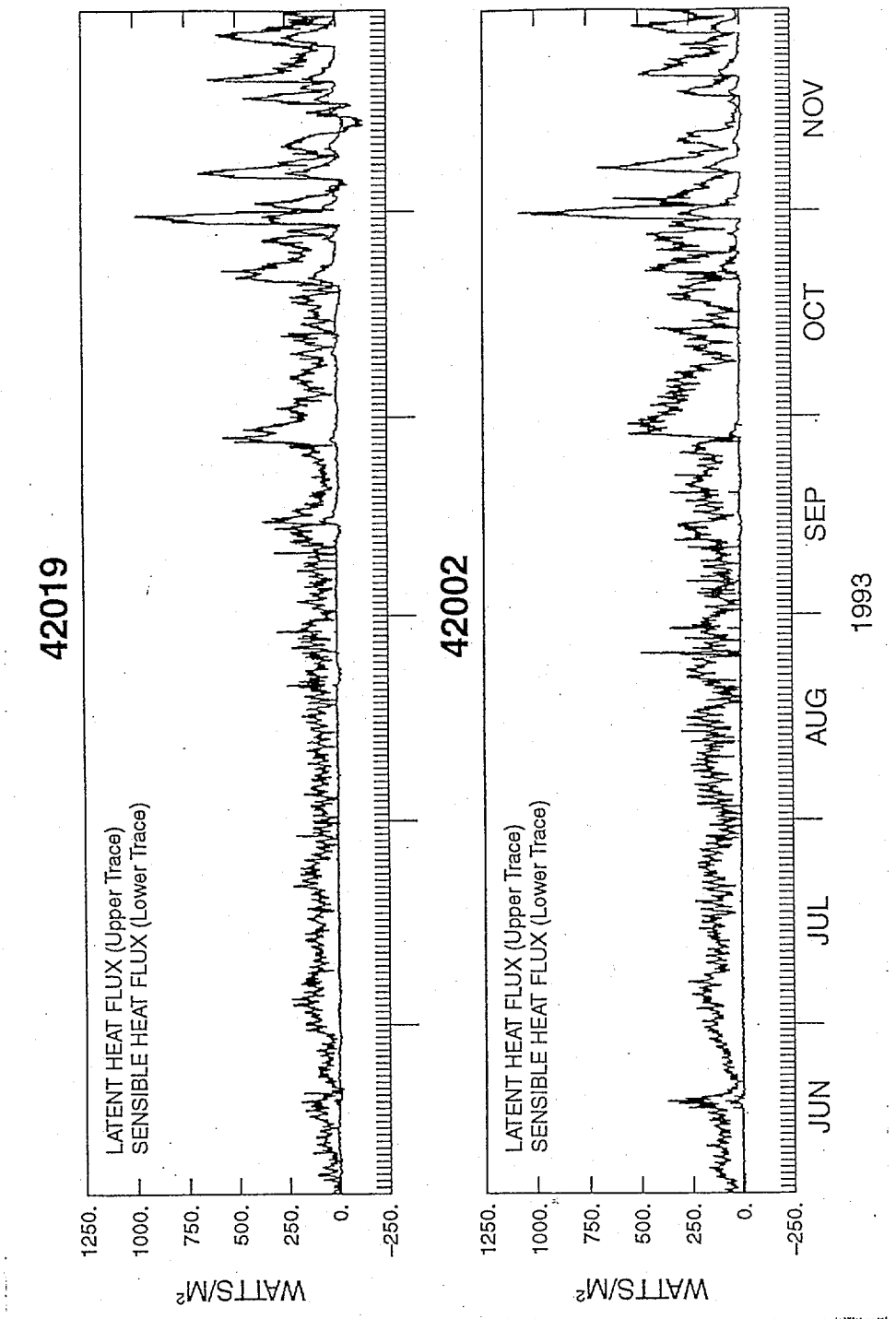

Figure 16. Hourly time series of latent (upper) and sensible (lower) heat fluxes are plotted for the buoy at station 42019 in the upper panel and likewise for 42002 in the lower panel. The record length is the same as for specific humidity.

The latent heat fluxes and the sensible heat fluxes for both buoys, when plotted together, are very similar and thus highly correlated (not shown). Plots of the Bowen ratio time series (ratio of the sensible-to-latent heat fluxes)t were also produced. The Bowen ratio was generally small (< ~0.1); however, occasional isolated spikes (*i.e.*, transient extreme values) occurred that were usually positive and exceeded 0.5 in several cases. These spikes occurred more frequently at 42002 and were distributed across the entire record; there were fewer spikes at 42019 and those that occurred, were observed only during October and November.

5. SUMMARY AND CONCLUSIONS

The overall reliability of the Rotronic MP-100 humidity sensors, which have been deployed on various NDBC buoys over the past five years, has improved significantly since 1989 when they were first considered for possible long-term deployment on fixed platforms at sea.

Over the approximate six-month period that the Rotronic sensor installed on the buoy at station 42019 was deployed, its calibration remained within the accuracy limits set by the WMO. The Rotronic sensor installed on the buoy at station 42002 has been operating continuously since its deployment in June 1993 (a period of more than 26 months).

Katsaros et al. (1994) have recently reported that the Rotronic sensor experiences hysteresis following periods of high mosture. Our observations did not permit us to examine this question in detail. In this regard, our results may not be representative of the results that might have been obtained elsewhere such as along the coast of Califronia where fog is frequently encountered. However, problems associated with hysteresis for the Rotronic sensor have not been reported elsewhere. Clearly, this issue needs further clarification. If hysteresis turns out to be a continuing problem that cannot be easily solved, moisture data from this instrument will most likely be unsuitable for research; however, it should still be of considerable value for operational applications.

During the six-month period of this study, most of the synoptic-scale variability that was encountered occurred after the first week in September and was due to the arrival of frontal systems with cold, dry air behind them that dropped down into the Gulf of Mexico from the continental U.S. One exception occurred in June when Tropical Storm Arlene moved NNW across the Gulf strongly influencing the moisture field in the vicinity of the buoys. In summary, the moisture-related parameters acquired at the buoys (specific humidity in particular) were highly sensitive in all cases to the various synoptic-scale events and to the seasonal variability that took place in the marine boundary layer during the period of this study.

Observations at each of the buoys acquired during this study were used to construct time series of specific humidity; in turn, from these and other supporting data, the surface

fluxes of latent and sensible heat were calculated. The time series of specific humidity at a height of 10 meters reveal three primary scales of variability:

- small-scale (of the order of hours),
- synoptic-scale (~several days), and
- seasonal (several months).

The synoptic-scale variability was clearly dominant and event-like in character; also, it occurred primarily during September, October and November.

A cross-correlation analysis between the buoys (for a separation distance of 263 km) for specific humidity and the other buoy parameters (at 10 meters) indicated:

- (1) all parameters were highly-correlated (> 0.9) except for wind speed,
- (2) the e-folding correlation distance for specific humidity was at least 800 km, and
- (3) specific humidity and air temperature both served as tracers of the motion associated with propagating atmospheric disturbances.

A more detailed cross-correlation analysis of the specific humidity time series revealed a major change in correlation structure that occurred during the first week in September indicating that weather patterns became more coherent and tended to enter the northern Gulf of Mexico from the North rather than from the South, as they tended to prior to this time.

Autospectra of the various buoy measurements revealed strong diurnal and semidiurnal variability for barometric pressure and SST and lesser variability at these periods for air temperature and wind speed. Also, weaker synoptic-scale variability was evident at periods of 3-4 days for most of the atmospheric parameters.

Analysis of the surface wave observations from each buoy included calculations of wave age and surface roughness. The results are consistent with enhanced moisture transfer between the ocean and the marine boundary layer during periods of high latent heat flux.

The surface fluxes of latent and sensible heat were dominated by the synoptic events which took place after mid-September. Sharp, positive maxima in these fluxes coincided with the arrival of these transient events in the northern Gulf of Mexico. The predominant direction of heat transfer for both fluxes was from the ocean to the atmosphere (~100% of the time for the latent heat fluxes, and 60 and 97% of the time for the sensible heat fluxes for buoys 42019 and 42002, respectively). The latent heat fluxes usually far exceeded the sensible heat fluxes as indicated by mean Bowen ratios of 6.3% at buoy 42019 and 8.3% at buoy 42002.

ACKNOWLEDGEMENTS

We take this opportunity to thank Bhavani Balashubramaniyan and Rachel Teboulle for constructing many of the figures contained in the text. We thank Steve Lord for creating figure 8 and for reviewing the text. We thank Lech Lobocki for providing technical assistance during the course of this study. Finally, we thank D. B. Rao, Ted Mettlach, Eric Meindl and Ed Michelena for providing reviews fo the text.

REFERENCES

Coantic, M., and C. A. Friehe, 1980: Slow-response humidity sensors. *Air-Sea Interaction, In Instruments and Methods* (F. Dobson, L. Hasse, and R. Davis, eds.) Plenum Press, New York and London, pp 399-411.

Crane, J., and D. Boole, 1988: Thin film humidity sensors: a rising technology. *Sensors*, **5**, 32-35.

Crescenti, G. H., R. E. Payne, and R. A. Weller, 1990: Improved meteorological measurements from buoys and ships (IMET): preliminary comparison of humidity sensors. *Woods Hole Tech. Rep. WHOI-90-18*, Woods Hole Oceanographic Institution, 57 pp.

Fairall, C. W., J. B. Edson, and M. A. Miller, 1990: Heat fluxes, whitecaps, and sea spray. *Surface Waves and Fluxes,* Volume **1** - *Current Theory* (G.L. Geernaert, and W. J. Plant, eds.) Kluwer Academic Publishers, Dordrecht, pp 173-208.

Friehe, C. A., and K. F. Schmitt, 1976: Parameterization of air-sea interface fluxes of sensible heat and moisture by the bulk aerodynamic formulas. *J. Phys. Oceanogr.*, **6**, 801-809.

Gill, A. E., 1982: Atmosphere-Ocean Dynamics, *International Geophysics Series,* Volume **30**. New York: Academic Press, 662 pp.

Hundermark, B. W., 1989: Field evaluation of the Rotronic humidity sensor and the impulsphysik visibility sensor. *Proceedings*, Conference and Exposition on Marine Data Sysytems, New Orleans, Louisiana, Marine Technology Society, 81-85.

IMSL, Inc., 1982: *IMSL Library Reference Manual*, ed. 8, vol. **2**, Houston, Texas.

Katsaros, K. B., J. DeCosmo, R. J. Lind, R. J. Anderson, S. D. Smith, R. Kraan, W. Oost, K. Uhlig, P. G. Mestayer, S. E. Larsen, M. H. Smith, and G. de Leeuw, 1994: Measurements of humidity and temperature in the marine environment during the HEXOS main experiment. *J. Atmos. Oceanic Technol.*, **11**, 964-981.

Kraus, E. B., 1972: *Atmosphere - Ocean Interaction*, Clarendon Press, Oxford , 275 pp.

Muller, S. A. and P. J. Beekman, 1987: A test of commercial humidity sensors for use at automatic weather stations. *J. Atmos. Oceanic Technol.*, **4**, 731-735.

Perry, A. H. and J. M. Walker, 1977: *The Ocean - Atmosphere System*, Longman, New York, 160 pp.

Phillips, O. M., 1958: The equilibrium range in the spectrum of wind-generated waves. *J. Fluid Mech.*, **4**, 426-434.

Pierson, W. J. and L. Moskowitz, 1964: A proposed spectral form for fully-developed wind seas based on the similarity theory of S. A. Kitaigorodskii. *J. Geophys. Res.*, **69**: 5181-5190.

Roll, H. U., 1965: Physics of the Marine Atmosphere, *International Geophysics Series*, Volume **7**, Academic Press, New York, 426 pp.

Semmer, S. R., 1987: Evaluation of a capacitance humidity sensor. *Sixth Symposium on Meteorological Observations and Instrumentation*, New Orleans, Louisiana, American Meteorological Society, 223-225.

Talley, L. D., 1984: Meridional heat transport in the Pacific ocean. *J. Phys. Oceanogr.*, **14** 231- 241.

Visscher, G. J. W. and K. Schurer, 1985: Some research on the stability of several capacitive thin film (polymer) humidity sensors in practice. *Proceedings,* International Symposium on Moisture and Humidity, Washington, D.C., Instrument Society of America, 515-523.

Van der Meulen, J. P., 1988: On the need of appropriate filter techniques to be considered using electrical humidity sensors. *Proc. WMO Technical Conf. on Instruments and Methods of Observation (TECO-1988)*, Leipzig, Germany, WMO, 55-60.

World Meteorological Organization, 1983: Measurement of Atmospheric humidity. *Guide to Meteorological Instruments and Methods of Observation*, Fifth Edition. WMO No. 8.

Wu, J., 1974: Evaporation due to spray. *J. Geophys. Res.*, **79**, 4107-4109.

No. 21. Breaker, L. C., 1989: El Nino and Related Variability in Sea-Surface Temperature Along the Central California Coast. PACLIM Monograph of Climate Variability of the Eastern North Pacific and Western North America, Geophysical Monograph 55, AGU, 133-140.

No. 22. Yu, T. W., D. C. Esteva, and R. L. Teboulle, 1991: A Feasibility Study on Operational Use of Geosat Wind and Wave Data at the National Meteorological Center. Technical Note/NMC Office Note No. 380, 28pp.

No. 23. Burroughs, L. D., 1989: Open Ocean Fog and Visibility Forecasting Guidance System. Technical Note/NMC Office Note No. 348, 18pp.

No. 24. Gerald, V. M., 1987: Synoptic Surface Marine Data Monitoring. Technical Note/NMC Office Note No. 335, 10pp.

No. 25. Breaker, L. C., 1989: Estimating and Removing Sensor Induced Correlation form AVHRR Data. Journal of Geophysical Reseach, 95, 9701-9711.

No. 26. Chen, H. S., 1990: Infinite Elements for Water Wave Radiation and Scattering. International Journal for Numerical Methods in Fluids, 11, 555-569.

No. 27. Gemmill, W. H., T. W. Yu, and D. M. Feit, 1988: A Statistical Comparison of Methods for Determining Ocean Surface Winds. Journal of Weather and Forecasting. 3, 153-160.

No. 28. Rao. D. B., 1989: A Review of the Program of the Ocean Products Center. Weather and Forecasting. 4, 427-443.

No. 29. Chen, H. S., 1989: Infinite Elements for Combined Diffration and Refraction . Conference Preprint, Seventh International Conference on Finite Element Methods Flow Problems, Huntsville, Alabama, 6pp.

No. 30. Chao, Y. Y., 1989: An Operational Spectral Wave Forecasting Model for the Gulf of Mexico. Proceedings of 2nd International Workshop on Wave Forecasting and Hindcasting, 240-247.

No. 31. Esteva, D. C., 1989: Improving Global Wave Forecasting Incorporating Altimeter Data. Proceedings of 2nd International Workshop on Wave Hindcasting and Forecasting,Vancouver, B.C., April 25-28, 1989, 378-384.

No. 32. Richardson, W. S., J. M. Nault, and D. M. Feit, 1989: Computer-Worded Marine Forecasts. Preprint, 6th Symp. on Coastal Ocean Management Coastal Zone 89, 4075-4084.

No. 33. Chao, Y. Y., and T. L. Bertucci, 1989: A Columbia River Entrance Wave Forecasting Program Developed at the Ocean Products Center. Techical Note/NMC Office Note 361.

No. 34. Burroughs, L. D., 1989: Forecasting Open Ocean Fog and Visibility. Preprint, 11th Conference on Probability and Statisitcs, Monterey, Ca., 5pp.

No. 35. Rao, D. B., 1990: Local and Regional Scale Wave Models. Proceeding (CMM/WMO) Technical Conference on Waves, WMO, Marine Meteorological of Related Oceanographic Activities Report No. 12, 125-138.

No. 36. Burroughs, L.D., 1991: Forecast Guidance for Santa Ana conditions. Technical Procedures Bulletin No. 391, 11pp.

No. 37. Burroughs, L. D., 1989: Ocean Products Center Products Review Summary. Technical Note/NMC Office Note No. 359. 29pp.

No. 38. Feit, D. M., 1989: Compendium of Marine Meteorological and Oceanographic Products of the Ocean Products Center (revision 1). NOAA Technical Memo NWS/NMC 68.

No. 39. Esteva, D. C., and Y. Y. Chao, 1991: The NOAA Ocean Wave Model Hindcast for LEWEX. Directional Ocean Wave Spectra, Johns Hopkins University Press, 163-166.

No. 40. Sanchez, B. V., D. B. Rao, and S. D. Steenrod, 1987: Tidal Estimation in the Atlantic and Indian Oceans, 3° x 3° Solution. NASA Technical Memorandum 87812, 18pp.

No. 41. Crosby, D. S., L. C. Breaker, and W. H. Gemmill, 1990: A Defintion for Vector Correlation and its Application to Marine Surface Winds. Technical Note/NMC Office Note No. 365, 52pp.

No. 42. Feit, D. M., and W. S. Richardson, 1990: Expert System for Quality Control and Marine Forecasting Guidance. Preprint, 3rd Workshop Operational and Metoerological. CMOS, 6pp.

No. 43. Gerald, V. M., 1990: OPC Unified Marine Database Verification System. Technical Note/NMC Office Note No. 368, 14pp.

No. 44. Wohl, G. M., 1990: Sea Ice Edge Forecast Verification System. National Weather Association Digest, (submitted)

No. 45. Feit, D. M., and J. A. Alpert, 1990: An Operational Marine Fog Prediction Model. NMC Office Note No. 371, 18pp.

No. 46. Yu, T. W., and R. L. Teboulle, 1991: Recent Assimilation and Forecast Experiments at the National Meteorological Center Using SEASAT-A Scatterometer Winds. Technical Note/NMC Office Note No. 383, 45pp.

No. 47. Chao, Y. Y., 1990: On the Specification of Wind Speed Near the Sea Surface. Marine Forecaster Training Manual.

No. 48. Breaker, L. C., L. D. Burroughs, T. B. Stanley, and W. B. Campbell, 1992: Estimating Surface Currents in the Slope Water Region Between 37 and 41°N Using Satellite Feature Tracking. Technical Note, 47pp.

No. 49. Chao, Y. Y., 1990: The Gulf of Mexico Spectral Wave Forecast Model and Products. Technical Procedures Bulletin No. 381, 3pp.

No. 50. Chen, H. S., 1990: Wave Calculation Using WAM Model and NMC Wind. Preprint, 8th ASCE Engineering Mechanical Conference, 1, 368-372.

No. 51. Chao, Y. Y., 1990: On the Transformation of Wave Spectra by Current and Bathymetry. Preprint, 8th ASCE Engineering Mechnical Conference, 1, 333-337.

No. 52. WAS NOT PUBLISHED

No. 53. Rao, D. B., 1991: Dynamical and Statistical Prediction of Marine Guidance Products. Proceedings, IEEE Conference Oceans 91, 3, 1177-1180.

No. 54. Gemmill, W. H., 1991: High-Resolution Regional Ocean Surface Wind Fields. Proceedings, AMS 9th Conference on Numerical Weather Prediction, Denver, CO, Oct. 14-18, 1991, 190-191.

No. 55. Yu, T. W., and D. Deaven, 1991: Use of SSM/I Wind Speed Data in NMC's GDAS. Proceedings, AMS 9th Conference on Numerical Weather Prediction, Denver, CO, Oct. 14-18, 1991, 416-417.

No. 56. Burroughs, L. D., and J. A. Alpert, 1993: Numerical Fog and Visiability Guidance in Coastal Regions. Technical Procedures Bulletin. No. 398, 6pp.

No. 57. Chen, H. S., 1992: Taylor-Gelerkin Method for Wind Wave Propagation. ASCE 9th Conf. Eng. Mech. (in press)

No. 58. Breaker, L. C., and W. H. Gemmill, and D. S. Crosby, 1992: A Technique for Vector Correlation and its Application to Marine Surface Winds. AMS 12th Conference on Probability and Statistics in the Atmospheric Sciences, Toronto, Ontario, Canada, June 22-26, 1992.

No. 59. Yan, X.-H., and L. C. Breaker, 1993: Surface Circulation Estimation Using Image Processing and Computer Vision Methods Applied to Sequential Satellite Imagery. Photogrammetric Engineering and Remote Sensing, 59, 407-413.

No. 60. Wohl, G., 1992: Operational Demonstration of ERS-1 SAR Imagery at the Joint Ice Center. Proceeding of the MTS 92 - Global Ocean Partnership, Washington, DC, Oct. 19-21, 1992.

No. 61. Waters, M. P., Caruso, W. H. Gemmill, W. S. Richardson, and W. G. Pichel, 1992: An Interactive Information and Processing System for the Real-Time Quality Control of Marine Meteorological Oceanographic Data. Pre-print 9th International Conference on Interactive Information and Processing System for Meteorology, Oceanography and Hydrology, Anaheim, CA, Jan. 17-22, 1993.

No. 62. Breaker, L. C., and V. Krasnopolsky, 1994: The Problem of AVHRR Image Navigation Revisited. Int. Journal of Remote Sensing, 15, 979-1008.

No. 63. Crosby, D. S., L. C. Breaker, and W. H. Gemmill, 1993: A Proposed Definition for Vector Correlation in Geophysics: Theory and Application. Journal of Atmospheric and Ocean Technology, 10, 355-367.

No. 64. Grumbine, R., 1993: The Thermodynamic Predictability of Sea Ice. Journal of Glaciology, 40, 277-282, 1994.

No. 65. Chen, H. S., 1993: Global Wave Prediction Using the WAM Model and NMC Winds. 1993 International Conference on Hydro Science and Engineering, Washington, DC, June 7 - 11, 1993. (submitted)

No. 66. WAS NOT PUBLISHED

No. 67. Breaker, L. C., and A. Bratkovich, 1993: Coastal-Ocean Processes and their Influence on the Oil Spilled off San Francisco by the M/V Puerto Rican. Marine Environmental Research, 36, 153-184.

No. 68. Breaker, L. C., L. D. Burroughs, J. F. Culp, N. L. Gunasso, R. Teboulle, and C. R. Wong, 1993: Surface and Near-Surface Marine Observations During Hurricane Andrew. Technical Note/NMC Office Note #398, 41pp.

No. 69. Burroughs, L. D., and R. Nichols, 1993: The National Marine Verification Program - Concepts and Data Management, Technical Note/NMC Office Note #393, 21pp.

No. 70. Gemmill, W. H., and R. Teboulle, 1993: The Operational Use of SSM/I Wind Speed Data over Oceans. Pre-print 13th Conference on Weather Analyses and Forecasting, AMS Vienna, VA., August 2-6, 1993, 237-238.

No. 71. Yu, T.-W., J. C. Derber, and R. N. Hoffman, 1993: Use of ERS-1 Scatterometer Backscattered Measurements in Atmospheric Analyses. Pre-print 13th Conference on Weather Analyses and Forecasting, AMS, Vienna, VA., August 2-6, 1993, 294-297.

No. 72. Chalikov, D. and Y. Liberman, 1993: Director Modeling of Nonlinear Waves Dynamics. J. Physical, (To be submitted).

No. 73. Woiceshyn, P., T. W. Yu, W. H. Gemmill, 1993: Use of ERS-1 Scatterometer Data to Derive Ocean Surface Winds at NMC. Pre-print 13th Conference on Weather Analyses and Forecasting, AMS, Vienna, VA, August 2-6, 1993, 239-240.

No. 74. Grumbine, R. W., 1993: Sea Ice Prediction Physics. Technical Note/NMC Office Note #396, 44pp.

No. 75. Chalikov, D., 1993: The Parameterization of the Wave Boundary Layer. Journal of Physical Oceanography, Vol. 25, No. 6, Par 1, 1333-1349.

No. 76. Tolman, H. L., 1993: Modeling Bottom Friction in Wind-Wave Models. Ocean Wave Measurement and Analysis, O.T. Magoon and J.M. Hemsley Eds., ASCE, 769-783.

No. 77. Breaker, L., and W. Broenkow, 1994: The Circulation of Monterey Bay and Related Processes. Oceanography and Marine Biology: An Annual Review, 32, 1-64.

No. 78. Chalikov, D., D. Esteva, M. Iredell and P. Long, 1993: Dynamic Coupling between the NMC Global Atmosphere and Spectral Wave Models. Technical Note/NMC Office Note #395, 62pp.

No. 79. Burroughs, L. D., 1993: National Marine Verification Program - Verification Statistics - Verification Statistics, Technical Note/NMC Office Note #400, 49 pp.

No. 80. Shashy, A. R., H. G. McRandal, J. Kinnard, and W. S. Richardson, 1993: Marine Forecast Guidance from an Interactive Processing System. 74th AMS Annual Meeting, January 23 - 28, 1994.

No. 81. Chao, Y. Y., 1993: The Time Dependent Ray Method for Calculation of Wave Transformation on Water of Varying Depth and Current. Wave 93 ASCE.

No. 82. Tolman, H. L., 1994: Wind-Waves and Moveable-Bed Bottom Friction. Journal of Physical Oceanography, 24, 994-1009.

No. 83. Grumbine, R. W., 1993: Notes and Correspondence A Sea Ice Albedo Experiment with the NMC Meduim Range Forecast Model. Weather and Forecasting, (submitted).

No. 84. Chao, Y. Y., 1993: The Gulf of Alaska Regional Wave Model. Technical Procedure Bulletin, No. 427, 10 pp.

No. 85. Chao, Y. Y., 1993: Implementation and Evaluation of the Gulf of Alaska Regional Wave Model. Technical Note, 35 pp.

No. 86. WAS NOT PUBLISHED.

No. 87. Burroughs, L., 1994: Portfolio of Operational and Development Marine Meteorological and Oceanographic Products. Technical Note/NCEP Office Note No. 412, 52 pp. [PB96-158548]

No. 88. Tolman, H. L., and D. Chalikov, 1994: Development of a third-generation ocena wave model at NOAA-NMC. Proc. Waves Physical and Numberial Modelling, M. Isaacson and M.C. Quick Eds., Vancover, 724-733.

No. 89. Peters, C., W. H. Gemmill, V. M. Gerald, and P. Woiceshyn, 1994: Evaluation of Empirical Transfer Functions for ERS-1 Scatterometer Data at NMC. 7th Conference on Satellite Meteorology and Oceanography, June 6-10, 1994, Monterey, CA., pg. 550-552.

No. 90. Breaker, L. C., and C. R. N. Rao, 1996: The Effects of Aerosols from the Mt. Pinatubo and Mt. Hudson Volcanio Eruption on Satellite-Derived Sea Surface Temperatures. Journal of Geophysical Research. (To be submitted).

No. 91. Yu, T-W., P. Woiceshyn, W. Gemmill, and C. Peters, 1994: Analysis & Forecast Experiments at NMC Using ERS-1 Scatterometer Wind Measurements. 7th Conference on Satellite Meteorology and Oceanography, June 6-10, 1994, Monterey, CA., pg. 600-601.

No. 92. Chen, H. S., 1994: Ocean Surface Waves. Technical Procedures Bulletin, No. 426, 17 pp.

No. 93. Breaker, L. C., V. Krasnopolsky, D. B. Rao, and X.-H. Yan, 1994: The Feasibility of Estimating Ocean Surface Currents on an Operational Basis using Satellite Feature Tracking Methods. Bulletin of the American Meteorolgical Society, 75, 2085-2095.

No. 94. Krasnopolsky V., L. C. Breaker, and W. H. Gemmill, 1994: Development of Single "All-Weather" Neural Network Algorithms for Estimating Ocean Surface Winds from the Special Sensor Microwave Imager. Technical Note.

No. 95. Breaker, L. C., D. S. Crosby and W. H. Gemmill, 1994: The application of a New Definition for Vector Correlation to Problems in Oceanography and Meteorology. Journal of Applied Meteolorology, 33, 1354-1365.

No. 96. Peters, C. A., V. M. Gerald, P. M. Woiceshyn, and W. H. Gemmill, 1994: Operational Processing of ERS-1 Scatterometer winds: A Documentation. Technical Note.

No. 97. Gemmill, W. H., P. M. Woiceshyn, C. A. Peters, and V. M. Gerald, 1994: A Preliminary Evaluation Scatterometer Wind Transfer Functions for ERS-1 Data. Technical Note.

No. 98. Chen, H. S., 1994: Evaluation of a Global Ocean Wave Model at NMC. International Conference on Hydro-Science and Engineering. Beijing, China, March 22 - 26, 1995.

No. 99. Aikman, F. and D. B. Rao, 1994: NOAA Perspective on a Coastal Forecast System.

No. 100. Rao, D. B. and C. Peters, 1994: Two-Dimensional Co-Oscillations in a Rectangular Bay: Possible Application to Water Problems. Marine Geodesy, 18, 317-332.

No. 101. Breaker, L. C., L. D. Burroughs, Y. Y. Chao, J. F. Culp, N. L. Gunasso, R. Teboulle, and C. R. Wong, 1994: Surface and Near-Surface Marine Observations During Hurricane Andrew. Weather and Forecasting, 9, 542-556.

No. 102. Tolman, H. L., 1995: Subgrid Modeling of Moveable-bed Bottom Friction in Wind Wave Models. Coastal Engineering, (in press).

No. 103. Breaker, L. C., D. B. Gilhousen, H. L. Tolman and L. D. Burroughs, 1995: Initial Results from Long-Term Measurements of Atmospheric Humidity and Related Parameters the Marine Boundary Layer at Two Locations in the Gulf of Mexico. (To be submitted to Global Atmosphere and Ocean Systems).

No. 104. Burroughs, L. D., and J. P. Dallavalle, 1995: Great Lakes Wind and Wave Guidance. Technical Procedures Bulletin No., (In preparation).

No. 105. Burroughs, L. D., and J. P. Dallavalle, 1995: Great Lakes Storm Surge Guidance. Technical Procedures Bulletin No., (In preparation).

No. 106. Shaffer, W. A., J. P. Dallavalle, and L. D. Burroughs, 1995: East Coast Extratropical Storm Surge and Beach Erosion Guidance. Technical Procedures Bulletin No., (In preparation)

No. 107. WAS NOT PUBLISHED.

No. 108. WAS NOT PUBLISHED.

No. 109. WAS NOT PUBLISHED.

No. 110. Gemmill, W. H, and C. A. Peters, 1995: The Use of Satellite Dervired Wind Data in High-Resolution Regional Ocean Surface Wind Fields. Conference on Coastal Oceanic and Atmospheric Prediction, Jan 28 - Feb 2, 1996, Atlanta, GA (accepted at preprint press).

OPC CHANGES TO OMB

No. 111. Krasnopolsky, V. M, W. H. Gemmill, and L. C. Breaker, 1995: Improved SSM/I Wind Speed Retrievals at Higher Wind Speeds. Journal of Geophysical Research, (in press).

No. 112. Chalikov, D., L. D. Breaker, and L. Lobocki, 1995: A Simple Model of Mixing in the Upper Ocean. Journal of Physical Ocean, (in press).

No. 113. Tolman, H. L., 1995: On the Selection of Propagation Schemes for a Spectral Wind-Wave Model. NCEP Office Note No. 411.

No. 114. Grumbine, R. W., 1995: Virtual Floe Ice Drift Forecast Model Intercomparison. NCEP Office Note. (To be submitted).

No. 115. Grumbine, R. W., 1995: Sea Ice Forecast Model Intercomparison: Selecting a Base Model for NCEP Sea Ice Modelling. Technical Note.

No. 116. Yu, T. W. and J. C. Derber, 1995: Assimilation Experiments with ERS-1 Winds: Part I - Use of Backscatter Measurements in the NMC Spectral Statistical Analysis System. Technical Note.

No. 117. Yu, T. W., 1995: Assimilation Experiments with ERS1 Winds: Part II - Use of Vector Winds in NCEP Spectral Statistical Analysis System. Technical Note.

No. 118. Grumbine, R. W., 1995: Sea Ice Drift Guidance. Technical Procedures Bulletin. (submitted)

No. 119. Tolman, H. L., 1996: Statistical Model Validation Techniques Applied to Marine Wind Speed Analysis. Technical Note.

No. 120. Grumbine, R. W., 1996: Automated Passive Microwave Sea Ice Concentration Analysis at NCEP. Technical Note.

No. 121. Grumbine, R. W., 1996: Sea Ice Prediction Environment: Documentation. Technical Note.

No. 122. Tolman, H. L and D. Chalikov, 1996: On the Source Terms in a Third-Generation Wind Wave Model. Journal of Physical Oceanography. (To be submitted).

No. 123. Gemmill, W. H., V. Krasnopolsky, L. C. Breaker, and C. Peters, 1996: Developments to Improve Satellite Derived Ocean Surface Winds for use in Marine Analyses. Pre-print Numerical Weather Prediction Conference, Norfolk, VA, Aug. 19-23, 1996 (To be submitted).

No. 124. Breaker, L. C., D. B. Gilhousen, H. L. Tolman and L. D. Burroughs, 1996: Initial Results from Long-Term Measurements of Atmospheric Humidity and Related Parameters in the Marine Boundary Layer at Two Locations in the Gulf of Mexico. NCEP Office Note No. 414.

No. 125. Yu, T. W., M. D. Iredell, and Y. Zhu, 1996: The Impact of ERS-1 Winds on NCEP Operational Numerical Weather Analyses and Forecast. Pre-print Numerical Weather Predicition Conference, Norfolk, VA, August 19-23, 1996. (To be submitted).

No. 126. Burroughs, L. D., 1996: Marine Meteorological and Oceanographic Guidance Products from the National Centers for Environmental Prediction. Mariners Weather Log. (To be submitted).

No. 127. Lobocki, L., 1996: Coastal Ocean Forecasting System (COFS) System Description and User Guides. Technical Note.

No. 128. Chalikov, D. and D. Sheinin, 1996: Direct Modeling of 1-D Nonlinear Potential Waves. Journal of Fluid Mechanics.

No. 129. Chalikov, D., 1996: A Global Ocean Model. Technical Note.

No. 130. Yu, T.W., 1996: Applications of SSM/I Wind Speed Data to NCEP Regional Analyses. Technical Note.


DEPARTMENT OF COMMERCE
UNITED STATES OF AMERICA